

Hydrodynamic cumulation mechanism caused by quantum shell effectsS. E. Kuratov , I. S. Menshov , S. Yu. Igashov, E. M. Urvachev , S. I. Blinnikov , D. S. Shidlovski, and S. I. Glazyrin 
Dukhov Research Institute of Automatics (VNIIA), Moscow 127055, Russia (Received 20 June 2023; revised 24 August 2023; accepted 14 September 2023; published 11 October 2023)

The computational and theoretical analysis carried out in this article demonstrates the existence of a nontrivial mechanism for the compression of a submicron-sized gas bubble formed by a gas of classical ions and a gas of degenerate electrons. This mechanism fundamentally differs from conventional compression mechanisms. It is shown that taking into account the quantum effect of a large spatial scale in the distribution of electrons qualitatively changes the character of cumulative processes. Because of a large-scale electric field caused by quantum shell effects, the compression process is characterized by the formation of multiple shock waves. The values of gas temperature and pressure achieved during compression occur higher by two orders of magnitude as compared with the classical adiabatic regime. The analysis is carried out within the framework of the following model: the dynamics of the electron subsystem is described by equations of a quantum electron fluid, while the hydrodynamic approximation is adopted for the ionic subsystem. The large-scale effect is taken into account by means of effective external field acting on electrons. The theoretical analysis carried out within this approach clarifies the nature of the cumulative process in the system under consideration; some quantitative characteristics obtained with numerical simulation are presented. The possibility of experimental observation of this cumulative mechanism is analyzed. It is suggested that the manifestation of the effect can be observed during laser compression of a system of submicron targets by measuring the neutron yield.

DOI: [10.1103/PhysRevE.108.045203](https://doi.org/10.1103/PhysRevE.108.045203)**I. INTRODUCTION**

One of the most promising methods to realize controlled thermonuclear fusion (CTF) is an inertial confinement fusion (ICF). This approach is based on the shell deuterium-tritium (DT) target implosion caused by x-ray radiation in a hohlraum at the NIF facility (USA) [1–3] and Laser Megajoule (France) [4], or direct laser irradiation at the Russia megajoule facility [5,6], or some other sources [7–9]. All of these ways suggest the classical hydrodynamic compression idea. The ablation of the outer target's shell produces several implosive shock waves that cumulate with the formation of a hot and dense region (hot spot) in the target center, where thermonuclear fusion starts. Despite recent record-breaking experiments at NIF [3] CTF is still far from being successfully implemented. An optimal target compression regime is one of the key issues in ICF. Consideration of some nontrivial but often omitted effects may improve our understanding of the cumulation process or even help us to propose alternate regimes of cumulation. An example of nontrivial effects is macroscopic quantum phenomena [10–12], which should be included in hydrodynamics simulation to find another way to realize CTF.

Previously, in Refs. [13,14], a unique nontrivial manifestation of quantum effects in a spherical mesoscopic system of degenerate electrons (with a number of electrons $N_e \sim 10^4 - 10^9$) was demonstrated. An unexpected absence of the simple tendency toward a uniform distribution of the electron density was found, which was tacitly assumed in the limit of large N_e . It has been shown that the electron density has a large spatial scale which is of the order of the system size and is much larger than another spatial scale—the Fermi wavelength of the electron gas. This large-scale effect clearly manifests

itself in the appearance of an electric field acting on the ionic system. The spatial distribution of the potential has an oscillating behavior with several extrema.

One of the possible manifestations of this effect is a nontrivial mode of compression of gas bubbles containing a mixture of a gas of degenerate electrons and a gas of classical ions, which is fundamentally different from the conventional gas compression. This circumstance was pointed out in [13]. The spherical symmetry of the system or proximity to it is of fundamental importance for the appearance of the effect.

Most research in the ICF areas is devoted to the compression of millimeter-sized targets. However, quantum effects show up best on submicron scales. Thus, in the present work, we investigate the hydrodynamic processes occurring during the compression of a nanoscale gas bubble with the effect of a large-scale spatially oscillating electric field. We will show that in such a regime the gas temperature and density in the hot-spot region is two orders of magnitude higher than without taking into account quantum effects. This increment can lead to launching thermonuclear fusion.

This paper is organized as follows. In Sec. I, we provide the approximate model that describes the hydrodynamics with the discussed effect. In Sec. II, we present both analytical and numerical investigation of such a system. In the Conclusion, we also discuss the possibility of the experimental confirmation of this effect.

II. FORMULATION OF THE MODEL

The common way of describing ICF-target dynamics is a hydrodynamics approach accounting for some process, e.g., radiation transfer, thermal conduction, thermonuclear

reactions, electron-ion interaction, and some other plasma effects. Here we adopt such an approach for consideration of a cumulation accounting for the quantum effect that leads to the emergence of a macroscopic spatial scale in the electron distribution.

The object to be studied is a submicron-sized hydrogen bubble formed by a gas of degenerate electrons ($\varepsilon_F > 0.1$ kT) and a gas of classical ions. Such conditions can be realized in the range of pressure values $p \sim 0.1 - 2$ TPa and temperature $T < 1$ eV.

Under these assumptions, the radius of the bubble R satisfies the following inequality:

$$\frac{R}{V_F^e} \ll \frac{1}{N^{\frac{1}{3}} V_i},$$

where V_F^e is the Fermi velocity of electrons, N is the number of electrons, and V_i is the ion velocity. This condition provides instant adjustment of the electronic subsystem to the profile of the ionic subsystem. That is, each current profile of the spatial distribution of ions corresponds to a certain spatial distribution of electrons. The emerging nonzero electric field acts on the ionic subsystem as a spatially distributed force. The ionic subsystem is compressing under this force and also an external force is applied to the outer surface of the bubble. Since the mean free path of ions is much less than the characteristic size of the system, their motion can be described in the hydrodynamic approximation taking into account an external force that depends on the ion concentration.

The problem is studied at a high concentration of particles, $n_e = 10^{24}$ cm $^{-3}$, or more so that the hydrogen atoms (to be considered) are so close to each other that the screening radius becomes smaller than the Bohr radius and the bound electron states disappear [15]. Therefore, under such conditions, hydrogen is completely ionized and is in the metallic state (Mott transition). This justifies the calculation of electron density distribution in the framework of the density functional theory (DFT) method using the ‘‘jelly’’ model in which ions are approximately represented as a continuous homogeneous distribution of positive charge and electrons are not bound to ions as they are in ordinary metals. Thus, to simulate accurately the compression of the gas bubble, it is necessary to solve self-consistently the following three problems (self-consistent formulation of the model):

(1) the quantum mechanical problem of determining the distribution of electrons against the background of ions by the DFT method;

(2) determining the emerging electric field which forms a force acting on the ionic subsystem by solving the Laplace equation;

(3) the hydrodynamic problem of the motion of the ionic subsystem in the presence of the force.

Such statement of the problem is associated with significant computational complexities and requires vast computational resources due to the quantum mechanical part dealing with solving the Schrödinger equations for the mesoscopic number of electrons $N_e \sim 10^9$. The computation time in numerical simulations drastically increases as soon as it becomes necessary to make repeated calculations of the quantum mechanical task $\sim 10^3$ to $\sim 10^4$ times per one gas-dynamic step to ensure the required accuracy. Therefore, we use a simpler

problem statement where the hydrodynamic equations of a quantum electron fluid [16] are solved for the evolution of the electron subsystem rather than the quantum mechanical problem. Such an approach, for example, is successfully used in modeling a quantum electron gas in plasma [17–21] and in various semiconductor electronic devices [22–24]. The validity of this approach for the system analyzed in the present work is discussed below.

In Sec. II A, we propose a mathematical model that describes the hydrodynamic motion of the considered system. Section II B is devoted to the effective field which is introduced to take into account the large-scale effect. In Sec. II C, we justify our effective field estimations.

A. Mathematical model

The mathematical model of hydrodynamic motion to be considered consists of the following three parts.

(1) The system of equations that determines the distribution of electrons looks as follows:

$$\frac{\partial \rho_e}{\partial t} + \frac{1}{r^2} \frac{\partial}{\partial r} (r^2 \rho_e v_e) = 0, \quad (1)$$

$$\frac{\partial v_e}{\partial t} + v_e \frac{\partial v_e}{\partial r} = -\frac{1}{\rho_e} \frac{\partial p_e}{\partial r} - \frac{e}{m_e} \frac{\partial}{\partial r} (\varphi + U_{\text{eff}}), \quad (2)$$

$$\frac{d e_e}{d t} + p_e \frac{d(1/\rho_e)}{d t} = 0. \quad (3)$$

Here r is the distance from the origin, located in the center of the spherical bubble, φ is the electrostatic potential, p_e is the quantum-statistical pressure of the degenerate electron gas and e_e is its internal energy, ρ_e and v_e are density and velocity, and e and m_e are the charge and mass of an electron. Fundamentally, an interesting feature of this model is the presence of an effective field U_{eff} in the equations of motion for the electrons, which models the large-scale effect. It will be described in detail below in Sec. II B.

It should be noted that the Bohmian term,

$$\varphi_{\text{Bohm}} = \frac{\hbar^2}{2m_e \sqrt{n_e}} \nabla^2 \sqrt{n_e},$$

in the above equation of motion (2) for the electron quantum liquid was neglected due to its smallness compared to U_{eff} .

(2) The system of equations describing the ionic subsystem has the form

$$\frac{\partial \rho_i}{\partial t} + \frac{1}{r^2} \frac{\partial}{\partial r} (r^2 \rho_i v_i) = 0, \quad (4)$$

$$\frac{\partial v_i}{\partial t} + v_i \frac{\partial v_i}{\partial r} = -\frac{1}{\rho_i} \frac{\partial p_i}{\partial r} - \frac{e}{m_i} \frac{\partial}{\partial r} \varphi, \quad (5)$$

$$\frac{d e_i}{d t} + p_i \frac{d(1/\rho_i)}{d t} = 0. \quad (6)$$

where the notation is analogous to the system (1)–(3) and the subscript i indicates parameters related to ions. Here there is no effective field, because it affects electrons only.

(3) The Poisson equation which determines the force acting on the ionic system is

$$\Delta \varphi = \frac{e}{\varepsilon_0} (n_i - n_e). \quad (7)$$

The system of Eqs. (1)–(7) is greatly simplified as applied to the problem under study. We consider the compression of the gas bubble in the neutral condition when $n_i \cong n_e$ at any moment since the characteristic time of the motion of the ion subsystem is much greater than the relaxation time of the electron subsystem. Within this approximation, the system of Eqs. (1)–(7) can be rewritten as follows:

$$0 = -\frac{1}{\rho_e} \frac{\partial p_e}{\partial r} - \frac{e}{m_e} \frac{\partial}{\partial r} (\varphi + U_{\text{eff}}), \quad (8)$$

$$\frac{\partial \rho_i}{\partial t} + \frac{1}{r^2} \frac{\partial}{\partial r} (r^2 \rho_i v_i) = 0, \quad (9)$$

$$\frac{\partial v_i}{\partial t} + v_i \frac{\partial v_i}{\partial r} = -\frac{1}{\rho_i} \frac{\partial p_e}{\partial r} - \frac{1}{\rho_i} \frac{\partial p_i}{\partial r} - \frac{e}{m_i} \frac{\partial}{\partial r} (U_{\text{eff}}), \quad (10)$$

$$\frac{d e_i}{d t} + p_i \frac{d(1/\rho_i)}{d t} = 0. \quad (11)$$

In subsequent sections the system of Eqs. (9)–(11) is used for the analysis of cumulative processes during the compression of a submicron-sized gas bubble. Equation (8) is then used to determine the electrical potential, which, in turn, is important for substantiating the correctness of the used form of the effective potential. Below we consider the modeling of an effective potential.

B. Modeling of the effective potential U_{eff}

Quantum shell effects in the system under consideration appear as large-scale inhomogeneity in the spatial distribution of the electron gas. The proposed formalism of quantum hydrodynamics is intended for taking into account such features of spatial distribution in the description of a mesoscopic system of degenerate electrons. This is achieved by means of introduction of an external effective potential U_{eff} in the equations of electron motion (8): Accordingly, for the model considered, it is vitally important to determine correctly the shape of this potential.

The dependence of the potential on the radius r can be determined in terms of the density n_e^{free} of free degenerate electrons in the potential well that is calculated within the DFT method. The averaged distribution of the electron density $\langle n_e^{\text{free}} \rangle$ is then calculated based on n_e^{free} by means of a smoothing procedure that smears out small-scale density fluctuations (on scales of the order of the Fermi length) while preserving large-scale structures. The distribution $\langle n_e^{\text{free}} \rangle$ found in this way allows us to calculate U_{eff} with the aid of the following relation:

$$\frac{1}{\langle n_e^{\text{free}} \rangle} \frac{\partial p_e(\langle n_e^{\text{free}} \rangle)}{\partial r} = -e \frac{\partial}{\partial r} [U_{\text{eff}}(r)], \quad (12)$$

which results from Eq. (8) in the absence of an electric field, i.e., for $\varphi = 0$.

The smoothing procedure can be carried out in various ways detailed as follows. Previously, in [13,14] we calculated the electric potential of an electrically neutral system as a whole consisting of a noninteracting gas of free degenerate electrons and an ionic spatially homogeneous ball. The potential is conventionally calculated by numerical integration of the charge density represented by a set of values in the grid

nodes with the Green's function of the Laplace equation. After that the averaging is performed. Then, using the averaged potential, we determine the electron density from the Poisson equation. As a result, the electron concentration averaged over small-scale fluctuations is obtained.

Here we use a more straightforward method, consisting in direct averaging of the density found in the framework of a quantum mechanical calculation. Appendix A demonstrates the equivalence of the two averaging approaches and presents results of calculating $U_{\text{eff}}(r)$ within our method. Figures 14–18 (see Appendix A) represent the calculated values of the effective potential depending on the dimensionless factor $k_F R_0$ and normalized by the parameter $\frac{(3\pi)^{2/3}}{2^{5/3}} \frac{\hbar^2}{m R_0^2}$, where k_f is $\frac{p_f}{\hbar}$, \hbar is the Planck constant, and m is the mass of an electron.

The obtained results allow us to draw the following conclusion about the shape of $U_{\text{eff}}(r)$. The potential consists of two qualitatively different terms,

$$U_{\text{eff}}(r) = U_{\text{osc}}(r) + U_{\text{bar}}(r), \quad (13)$$

where $U_{\text{osc}}(r)$ is the effective oscillating potential acting in the almost bulk of the inner region of the bubble ($r < R_0$) excluding a thin “skin”—in the vicinity of its border $r = R_0$, while $U_{\text{bar}}(r)$ is the effective barrier potential. On the contrary, the latter is constant with high accuracy in the almost bulk of the inner region of the bubble ($r < R_0$) and is sharply changing in a narrow boundary region ($r \sim R_0$).

The shape of the potential $U_{\text{osc}}(r)$ has an oscillating character; it depends on the number of particles and has from one to three bumps. A certain periodicity in the shape of the potential can be observed, considering its dependence on the number of particles with a characteristic period approximately equal to $\Delta k_F R_0 \sim (1.3\text{--}1.4)$ (see Figs. 14–20 in Appendix A) The amplitude of the effective potential is proportional to $\frac{1}{R_0^2}$ and weakly depends on N (N is the total number of electrons).

The shape of the potential $U_{\text{bar}}(r)$ has a stepwise profile and practically does not depend on the number of particles. The amplitude of the potential $U_{\text{bar}}(r)$ is proportional to $\frac{1}{R_0}$.

The effective potential can be approximated by convenient simple analytical expressions (see Appendix B for details):

$$U_{\text{bar}}(r) = \frac{W}{1 + \exp\left(\frac{r - R_{\text{ws}}}{a}\right)},$$

$$U_{\text{osc}}(r) = \sum_m^M C_m \cos\left(\pi m \frac{r}{R_0}\right), \quad (14)$$

where R_{ws} , C_m , and a are the adjustable constants. These approximations are used in numerical simulations in Sec. III. In the next subsection we validate the described estimations.

C. Validation of the effective potential approach: Analytical estimates

Strictly speaking, an approach based on the introduction of an effective field is a kind of assumption, which has to be validated. In this subsection we show that the approximations defined in Sec. II B make it possible to obtain satisfactory quantitative results for the amplitudes of the main functions

obtained in [13] with extended calculations by the DFT method.

Firstly, we note that Appendix A presents the calculated electrostatic potential $\varphi_{\text{electr}}^{\text{free}}$ that arises in the electrically neutral system of a gas of degenerate noninteracting electrons and a spatially homogeneous ball of ions. Figures 20–22 (see Appendix A) show the results of averaging $\varphi_{\text{electr}}^{\text{free}}$. The averaged potential qualitatively coincides with $U_{\text{eff}}(r)$; it depends on the number of particles and has from one to three local bumps.

We introduce the following quantities characterizing the system considered:

$U_{\text{osc}}(r)$: effective oscillating potential;

$\varphi_{\text{electr}}^{\text{free}}$: electric potential of electrically neutral system composed of noninteracting electrons and a spatially homogeneous ball of ions;

$\varphi_{\text{electr}}^{\text{interact}}$: the same as above except that electrons are considered to be interacting [$\varphi_{\text{electr}}^{\text{interact}} = \varphi$ from Eq. (8)];

$\delta n^{\text{free}}(r)$: deviation from the average value of the electron density;

$\delta n^{\text{interact}}(r)$: the same as above except that electrons are considered to be interacting.

Then we proceed as follows. Using the simplest model for the electrostatic potential, $\varphi_{\text{electr}}^{\text{free}} = \varphi_{0 \text{ electr}}^{\text{free}} \sin(\alpha \frac{r}{R_0})$, $\alpha = 3\pi$, and the results of [13], we determine an analytical approximation for the amplitude U_0^{osc} of $U_{\text{osc}}(r)$ in the following way [$U_0^{\text{osc}} = C_3$ from Eq. (14)].

Assuming that in the bulk of the volume, the deviation of the electron density from the average value is small, we obtain

$$\langle n_e^{\text{free}} \rangle = n_0 + \delta n(r),$$

$$p_e = \frac{(3\pi^2)^{\frac{2}{3}} \hbar^2}{5 m_e} n_0^{\frac{5}{3}} = \frac{(3\pi^2)^{\frac{2}{3}} \hbar^2}{5 m_e} n_0^{\frac{5}{3}} \left(1 + \frac{5}{3} \frac{\delta n}{n_0} \right).$$

Substituting the resulting expression into Eq. (12), we find the relation connecting the functions $\delta n(r)$ and U_{osc} :

$$-eU_{\text{osc}}(r) = \frac{(3\pi^2)^{\frac{2}{3}} \hbar^2}{5 m_e} n_0^{\frac{2}{3}} \frac{5}{3} \frac{\delta n(r)}{n_0}. \quad (15)$$

Using the Poisson equation

$$\frac{1}{r^2} \frac{\partial}{\partial r} \left(r^2 \frac{\partial \varphi_{\text{electr}}}{\partial r} \right) = \frac{e}{\varepsilon_0} \delta n,$$

one can get

$$-\varphi_{0 \text{ electr}}^{\text{free}} \sin \frac{\alpha}{R_0} \left[\frac{2r \sin(\alpha \frac{r}{R_0}) + r^2 \frac{\alpha}{R_0} \cos(\alpha \frac{r}{R_0})}{r^2} \right] = \frac{e}{\varepsilon_0} \delta n.$$

From Eq. (15), we can then obtain the following expression for the amplitude of the oscillating part:

$$U_0^{\text{osc}} = \varphi_{0 \text{ electr}}^{\text{free}} \frac{(3\pi^2)^{\frac{2}{3}} \hbar^2}{3 e^2 m_e} \frac{\varepsilon_0}{n_0^{\frac{1}{3}}} \left(\frac{\alpha}{R_0} \right)^2.$$

Taking into account that according to DFT calculations $\varphi_{0 \text{ electr}}^{\text{free}} = 0.02 \frac{eN^{0.45}}{4\pi\varepsilon_0 R_0}$ [13], we finally get the following expression for the effective potential amplitude:

$$U_0^{\text{osc}} = 0.06 \frac{\hbar^2}{e m_e} \frac{N^{0.117}}{R_0^2} \frac{(3\pi^2)^{\frac{2}{3}}}{12\pi} \left(\frac{4}{3}\pi \right)^{1/3} \alpha^2. \quad (16)$$

This value is in good qualitative and quantitative agreement with the results obtained in Appendixes A and B.

Similarly, within the framework of the proposed approach Eqs. (8)–(11) with the aid of Eq. (16), one can calculate the amplitudes of other functions $\varphi_{\text{electr}}^{\text{interact}}$, $\delta n^{\text{free}}(r)$, and $\delta n^{\text{interact}}(r)$:

$$\delta n^{\text{interact}}(r) = 0.06 \frac{N^{0.117} \alpha^2}{4\pi R_0^2} n_0^{\frac{1}{3}},$$

$$\varphi_{0 \text{ electr}}^{\text{interact}} \sim 0.02 \frac{eN^{0.45} \alpha^2}{4\pi \varepsilon_0 R_0 \left(\frac{4}{3}\pi \right)^{1/3}},$$

$$\delta n^{\text{free}}(r) \sim 0.06 \frac{N^{0.45} \alpha^2}{4\pi R_0^3}.$$

These expressions also are in good agreement with the results obtained earlier in [13,14] for the amplitudes of the corresponding functions (see Figs. 4 and 9 in [13]).

Thus it is shown that the approach based on the hydrodynamic description of an electron gas taking into account the effective potential allows us to describe principal features of the system obtained within the DFT method. This proves the validity of the proposed approximate approach for the analysis of the system considered in the present article.

It is important to note that this simplification, however, took into account the fundamentally important, in this study, quantum effect, which is a consequence of the shell structure. Recall that as it was shown [13], the coordinate dependence of the electron density of a mesoscopic system exhibits certain inhomogeneities on a large spatial scale comparable to the size of the system itself. This feature is taken into account in the present study by introducing some effective potential into the hydrodynamic equations used to describe the quantum electron fluid. Note that the comparison with the results of more accurate models, including various versions of the DFT, made in Ref. [13] substantiates the possibility and effectiveness of such a simplification. The most significant advantages of this simplified approach are a significant reduction in computational time and, at the same time, the absence of the need to use huge computing resources. Moreover, with an increase in the number of particles in the system, the computational complexity of the presented approach does not increase so dramatically as is the case of conventional DFT approaches.

III. PECULIARITIES OF HYDRODYNAMIC CUMULATION CAUSED BY QUANTUM SHELL EFFECTS

In this section, a mechanism of hydrodynamic cumulation initiated by quantum shell effects is theoretically investigated within the framework of the model formulated above. We consider two different problems that demonstrate the basic mechanism of shock wave formation.

The first problem is related to the “relaxation process” in a gas bubble being initially at rest when the effective potential is instantaneously switched on.

The second problem is the “adiabatic compression process” of a gas bubble where the densities of electrons and ions are assumed to practically coincide and have initially a non-monotonic spatial density profile with several local extrema.

Any of the possible mechanisms of gas bubble compression can be represented as a combination of these two processes.

Theoretical analyses presented in Secs. III A and III B are aimed to separate study of the relaxation and adiabatic compression processes. Thus we reveal the causes of forming multiple shock waves and discuss conditions for the occurrence of this phenomenon. In Sec. III C we provide the results of numerical simulation which demonstrates quantitatively the influence of the large-scale effect on the temperature values reached during the cumulation process. This simulation takes into account both processes.

A. Process of relaxation

The first problem is related to the relaxation process in the system with a nonmoving boundary being initially at rest ($n_e = n_i = n_0 = \text{const}$), in which the effective potential is instantaneously switched on. Such a situation can be realized, for example, under impact action on a metal cluster, in which the initial crystal lattice of ions is transformed into a plasma state. The final result of the process is formation of the static equilibrium ($v_i = 0$) state of the system.

Relaxation process in the system is governed by the set of the following equations:

$$0 = -\frac{1}{\rho_e} \frac{\partial p_e}{\partial r} - \frac{e}{m_e} \frac{\partial}{\partial r} (\varphi + U_{\text{eff}}),$$

$$\frac{\partial \rho_i}{\partial t} + \frac{1}{r^2} \frac{\partial}{\partial r} (r^2 \rho_i v_i) = 0,$$

$$\frac{\partial v_i}{\partial t} + v_i \frac{\partial v_i}{\partial r} = -\frac{1}{\rho_i} \frac{\partial p_i}{\partial r} - \frac{1}{\rho_i} \frac{\partial p_e}{\partial r} - \frac{e}{m_i} \frac{\partial}{\partial r} (U_{\text{eff}}),$$

$$\frac{d e_i}{d t} + p_i \frac{d(1/\rho_i)}{d t} = 0,$$

$$p_e = \frac{(3\pi^2)^{\frac{2}{3}} \hbar^2}{5} n_e^{\frac{5}{3}},$$

$$p_i = n_i k T_i.$$

The first-order perturbation theory approximation reads

$$n(t) = n_0 + \Delta n(r, t),$$

$$v_i = \Delta v_i(r, t),$$

$$T_i = T_i^0 + \Delta T_i(r, t),$$

$$p_e = \frac{(3\pi^2)^{\frac{2}{3}} \hbar^2}{5} n_0^{\frac{5}{3}} \left(1 + \frac{5}{3} \frac{\Delta n}{n_0} \right).$$

As a result, the equations that govern the evolution of the system take the form

$$\frac{\partial \Delta n(r, t)}{\partial t} + \frac{\partial}{\partial r} [n_0 \Delta v_i(r, t)] + \frac{2}{r} [n_0 \Delta v_i(r, t)] = 0, \quad (17)$$

$$\frac{\partial \Delta v_i}{\partial t} = -\frac{k}{m_i} \frac{\partial \Delta T_i(r, t)}{\partial r} - \frac{k T_i^0}{m_i n_0} \frac{\partial \Delta n(r, t)}{\partial r} - \frac{1}{m_i n_0} \frac{(3\pi^2)^{\frac{2}{3}} \hbar^2}{3} n_0^{\frac{2}{3}} \frac{\partial \Delta n(r, t)}{\partial r} - \frac{e}{m_i} \frac{\partial}{\partial r} (U_{\text{eff}}), \quad (18)$$

$$\frac{3k}{2m_i} \left(\frac{\partial \Delta T_i}{\partial t} \right) - \frac{k T_i^0}{m_i n_0} \left(\frac{\partial \Delta n}{\partial t} \right) = 0. \quad (19)$$

The initial conditions are $\Delta n(r, 0) = 0$, $\Delta v_i(r, 0) = 0$, $\Delta T_i(r, 0) = 0$.

The inhomogeneous wave equation for $\Delta n(r, t)$ follows from Eqs. (17)–(19) straightforwardly:

$$\frac{\partial^2 \Delta n}{(\partial t)^2} - \frac{c_0^2}{r} \frac{\partial^2 (r \Delta n)}{(\partial r)^2} = \frac{e n_0}{m_i} \frac{1}{r} \frac{\partial^2 (r U_{\text{eff}})}{(\partial r)^2}, \quad (20)$$

where

$$c_0^2 = \frac{5k T_i^0}{3m_i} + \frac{1}{m_i} \frac{(3\pi^2)^{\frac{2}{3}} \hbar^2}{3} n_0^{\frac{2}{3}}.$$

Let us first consider the relaxation dynamics of the system caused by the oscillation potential, for which we adopt the simplest model form:

$$U_{\text{osc}}(r) = \frac{\beta}{[R(t)]^2} \cos \left[\alpha \frac{r}{R(t)} \right],$$

$$\beta = 0.02 \frac{\hbar^2}{e m_e} \sqrt[4]{N} \frac{(3\pi^2)^{\frac{2}{3}}}{12\pi} \left(\frac{4}{3} \pi \right)^{1/3} \alpha^2.$$

Taking into account the initial conditions, the solution to Eq. (20) has the form

$$\Delta n(r, t) = \frac{n_0 e}{m_i c_0^2 (R_0)^2} \beta \cos \left(\alpha \frac{r}{R_0} \right) \left[-1 + \cos \left(\alpha \frac{c_0 t}{R_0} \right) \right],$$

$$\Delta v_i = \frac{e}{c_0 m_i (R_0)^2} \beta \sin \left(\alpha \frac{r}{R_0} \right) \sin \left(\alpha \frac{c_0 t}{R_0} \right).$$

The obtained expressions imply the applicability of the perturbation theory for the nanometer range bubbles,

$$\frac{\Delta n}{n_0} = \frac{e}{m_i c_0^2} \frac{0.02 \frac{\hbar^2}{e m_e} \sqrt[4]{N} \frac{(3\pi^2)^{\frac{2}{3}}}{12\pi} \left(\frac{4}{3} \pi \right)^{1/3} \alpha^2}{(R_0)^2} \sim 10^{-1},$$

as well as the expression for the speed of sound,

$$c = c_0 + \frac{c_0}{3} \frac{e}{m_i c_0^2} \frac{\beta}{(R_0)^2} \cos \left(\alpha \frac{r}{R_0} \right) \left[-1 + \cos \left(\alpha \frac{c_0 t}{R_0} \right) \right]. \quad (21)$$

The formation of shock waves in the class of flows (21) is described in detail in the classical textbook [25]. The time of the shock wave formation in such a spherically symmetric system of radius R_0 is estimated as

$$t = \frac{R_0}{\pi c_0 \frac{\Delta n}{n_0}} \sim \frac{R_0 m_e m_i c_0^2 (R_0)^2}{c_0 \hbar^2 \sqrt[4]{N}}.$$

For the values of $R_0 \sim 1$ nm, this time is comparable with the time required for sound waves to propagate over a distance of the order of the gas bubble size which is about $t \sim 10^{-14}$ s. Thus a system of shock waves can be generated in nanometer gas bubbles, which can lead to a significant cumulation of compression.

The possibility of formation of shock waves in a bubble with internal content initially at rest is associated with the existence of an electrostatic potential $\varphi_0^{\text{interact}} \sim 0.02 \frac{eN^{0.45}\alpha^2}{4\pi\epsilon_0 R_0 (\frac{4}{3}\pi)^{1/3}}$ in the system at the initial moment, and accordingly, with the stored electrostatic energy, which is transformed into the kinetic energy of motion with velocity of the order

$$V \sim \sqrt{\frac{e^2}{\epsilon_0 m_i R_0}} \sim 10 \text{ km/s.}$$

Note that under conditions of spherical cumulation, the value of the velocity can grow significantly in the central regions of the bubble.

The above analysis demonstrates the formation of shock waves caused by the oscillatory part of the effective potential. Now we analyze the influence of the barrier potential on the cumulation mechanisms. The electrical charge

$$Q = en_0 4\pi (R_0)^2 \delta,$$

is distributed at the initial moment over a spherical boundary layer whose thickness δ is of the order of several interatomic distances. The following estimate,

$$E \sim \frac{Q^2}{4\pi\epsilon_0 R_0},$$

is obvious for the electrostatic energy associated with this charge distribution. This energy is transformed into the kinetic energy of the bubble ions:

$$K = \frac{\frac{4}{3}\pi (R_0)^3 m_i n_0 V^2}{2}.$$

From here, the estimate for the ion mass velocity V follows straightforwardly:

$$V \sim \sqrt{\frac{e^2 n_0^{1/3}}{\epsilon_0 m_i}} \sim 10 \text{ km/s.}$$

This analysis clarifies that a set of shock waves forms due to the presence of the effective potential in the system during the process of relaxation. The possibility of the formation of shock waves in a bubble with interior initially at rest is associated with the existence of an electrostatic potential in the system at the initial moment, and accordingly, the stored electrostatic energy, which transforms into the kinetic energy of motion.

B. Adiabatic compression process

In the second problem, the compression of the gas bubble with the boundary evolution $R(t) = R_0 - U_0 t$ is considered. The adiabatic compression mode is assumed. This implies the fulfillment of the following conditions: (i) The boundary velocity U_0 is much less than the speed of sound in the gas bubble, and (ii) the characteristic compression time t is much longer than the time R_0/C_0 of the propagation of the sound wave through the bubble. In contrast to the standard mode, we take into account the large-scale effect.

There exists an exact solution that describes the regime of classical adiabatic compression of this system in the absence

of an oscillatory potential:

$$\begin{aligned} \rho_i^0(t) &= \frac{M_{\text{gas}}}{\frac{4}{3}\pi [R(t)]^3}, \\ n_0(t) &= \frac{\rho_i^0(t)}{m_i}, \\ T_i^0(t) &= [\rho_i^0(t)]^{\frac{2}{3}} \frac{T_i^0(0)}{[\rho_i^0(0)]^{\frac{2}{3}}}, \\ u_i(r, t) &= -U_0 \frac{r}{R(t)}. \end{aligned}$$

The presence of the oscillatory potential is taken into account in the framework of the first-order perturbation theory approximation:

$$\begin{aligned} n(t) &= n_0(t) + \Delta n(r, t), \\ v_i &= u_i(r, t) + \Delta v_i(r, t), \\ T_i &= T_i^0(t) + \Delta T_i(r, t). \end{aligned}$$

Note that the unperturbed temperature $T_i^0(t)$ and concentration $n_0(t)$ depend on time here, in contrast to Sec. III A. In addition, the unperturbed velocity $u_i(r, t)$ is nonzero.

$$\begin{aligned} P_e &= \frac{(3\pi^2)^{\frac{2}{3}} \hbar^2}{5 m_e} n^{\frac{5}{3}} \\ &= \frac{(3\pi^2)^{\frac{2}{3}} \hbar^2}{5 m_e} n_0^{\frac{5}{3}} \left(1 + \frac{5}{3} \frac{\Delta n}{n_0}\right). \end{aligned}$$

Within this approximation, the equations of motion of ions become

$$\begin{aligned} 0 &= -\frac{1}{m_e n_0(t)} \frac{(3\pi^2)^{\frac{2}{3}} \hbar^2}{3 m_e} n_0^{\frac{2}{3}} \frac{\partial \Delta n(r, t)}{\partial r} \\ &\quad - \frac{e}{m_e} \frac{\partial}{\partial r} (U_{\text{eff}}) - \frac{e}{m_e} \frac{\partial}{\partial r} \varphi, \end{aligned} \quad (22)$$

$$\begin{aligned} \frac{\partial \Delta n(r, t)}{\partial t} + \frac{\partial}{\partial r} [n_0(t) \Delta v_i(r, t) + \Delta n(r, t) u_i(r, t)] \\ + \frac{2}{r} [n_0(t) \Delta v_i(r, t) + \Delta n(r, t) u_i(r, t)] = 0, \end{aligned} \quad (23)$$

$$\begin{aligned} \frac{\partial \Delta v_i}{\partial t} + u_i(r, t) \frac{\partial \Delta v_i}{\partial r} \\ = -\Delta v_i \frac{\partial u_i(r, t)}{\partial r} - \frac{k}{m} \frac{\partial \Delta T_i(r, t)}{\partial r} - \frac{k T_i^0(t)}{m n_0(t)} \frac{\partial \Delta n(r, t)}{\partial r} \\ - \frac{1}{m n_0(t)} \frac{(3\pi^2)^{\frac{2}{3}} \hbar^2}{3 m_e} n_0^{\frac{2}{3}} \frac{\partial \Delta n(r, t)}{\partial r} - \frac{e}{m_i} \frac{\partial}{\partial r} (U_{\text{eff}}), \end{aligned} \quad (24)$$

$$\begin{aligned} \frac{3k}{2m} \left[\frac{\partial \Delta T_i}{\partial t} + u_i(r, t) \frac{\partial \Delta T_i}{\partial r} \right] \\ - \frac{k T_i^0(t)}{m n_0(t)} \left[\frac{\partial \Delta n}{\partial t} + u_i(r, t) \frac{\partial \Delta n}{\partial r} \right] \\ = \frac{k}{m n_0} \frac{\partial n_0(t)}{\partial t} \left[-T_i^0(t) \frac{\Delta n}{n_0} + \Delta T \right] - \frac{u_i e}{m_i} \frac{\partial}{\partial r} \varphi. \end{aligned} \quad (25)$$

In the adiabatic compression mode, the profile $\Delta n(r, t)$ will adjust to the profile U_{eff} . Therefore, we attempt to look for a solution of the above system of equations in the form

$$\Delta n(r, t) = A(t) \cos \left[\alpha \frac{r}{R(t)} \right] + D(t) r \sin \left[\alpha \frac{r}{R(t)} \right], \quad (26)$$

$$\Delta T(r, t) = B(t) \cos \left[\alpha \frac{r}{R(t)} \right] + E(t) r \sin \left[\alpha \frac{r}{R(t)} \right], \quad (27)$$

$$\Delta v_i(r, t) = C(t) r \cos \left[\alpha \frac{r}{R(t)} \right] + F(t) r^2 \sin \left[\alpha \frac{r}{R(t)} \right]. \quad (28)$$

Within the ansatz (26)–(28), Eqs. (22)–(25) lead to the identical relations that are presented below.

Collecting the terms with $\cos[\alpha \frac{r}{R(t)}]$ we obtain

$$\begin{aligned} \frac{\partial A(t)}{\partial t} + 3 \left[n_0(t) C(t) - A(t) \frac{U_0}{R(t)} \right] &= 0, \\ -\frac{k}{m} B(t) - \frac{k T_i^0(t)}{m n_0(t)} A(t) - \frac{1}{m n_0(t)} \frac{(3\pi^2)^{\frac{2}{3}}}{3} \frac{\hbar^2}{m_e} n_0^{\frac{2}{3}} A(t) \\ - \frac{e}{m_i} \frac{\beta}{[R(t)]^2} &= 0, \\ \frac{3k}{2m} \left[\frac{\partial B(t)}{\partial t} \right] - \frac{k T_i^0(t)}{m n_0(t)} \left[\frac{\partial A(t)}{\partial t} \right] \\ &= \frac{k}{m n_0} \frac{\partial n_0(t)}{\partial t} \left[-T_i^0(t) \frac{A(t)}{n_0} + B(t) \right]. \end{aligned}$$

It follows from here that

$$\begin{aligned} C(t) &= 0, \quad B(t) \sim R(t) A(t) \sim \frac{1}{[R(t)]^2}, \\ A(t) &= \frac{0.06\alpha^2 N^{0.45}}{4\pi R_0^3}. \end{aligned}$$

We estimate the applicability of the perturbation theory as follows:

$$\frac{\Delta n}{n_0} \sim \frac{0.02\alpha^2}{N^{0.55}} \sim 0.05 \ll 1.$$

It is clear that the applicability condition holds with a large margin.

Similarly, collecting the terms with $\sin[\alpha \frac{r}{R(t)}]$ one obtains

$$\begin{aligned} \frac{\partial D}{\partial t} - A(t) \alpha \frac{U_0}{[R(t)]^2} + 4n_0(t) F(t) - 4D(t) \frac{U_0}{R(t)} &= 0, \\ -kE(t) - \frac{k T_i^0(t)}{n_0(t)} D(t) - \frac{1}{n_0(t)} \frac{(3\pi^2)^{\frac{2}{3}}}{3} \frac{\hbar^2}{m_e} n_0^{\frac{2}{3}} D(t) &= 0, \\ 3k \frac{\partial E(t)}{\partial t} - \frac{k T_i^0(t)}{n_0(t)} \left[\frac{\partial D(t)}{\partial t} \right] \\ &= \frac{k}{n_0} \frac{\partial n_0(t)}{\partial t} \left[-T_i^0(t) \frac{D(t)}{n_0} + E(t) \right], \\ + \frac{U_0}{R(t)} \left\{ \alpha \frac{\beta e}{[R(t)]^3} + \frac{1}{n_0(t)} \frac{(3\pi^2)^{\frac{2}{3}}}{3} \frac{\hbar^2}{m_e} n_0^{\frac{2}{3}} A(t) \frac{\alpha}{R(t)} \right\}. \end{aligned}$$

$$\text{Hence, we get } F(t) = \frac{0.06\alpha^3 U_0}{12R_0^2 N^{0.55}}.$$

Now let us estimate the time of the shock wave formation by considering the trajectory of the Lagrangian particle $r(t, r_0)$ with the initial coordinate. The equation of motion has the following form:

$$\frac{dr(t, r_0)}{dt} = u_i[r(t, r_0), t] + \Delta v_i[r(t, r_0), t].$$

Applying the method of successive approximations, we obtain

$$\begin{aligned} r(t, r_0) &= r^{(0)}(t, r_0) + r^{(1)}(t, r_0), \\ r(t, r_0) &= [R_0(0) - U_0 t] \frac{r_0}{R_0(0)} \\ &+ \frac{0.06\alpha^3}{12N^{0.55}} \frac{r_0^2}{[R_0(0)]^2} \cos \left[\alpha \frac{r_0}{R_0(0)} \right] \\ &\times [R_0(0) - U_0 t] \ln \left(\frac{[R_0(0) - U_0 t]}{R_0(0)} \right). \end{aligned}$$

The condition for the occurrence of a shock wave is the intersection of the trajectories of Lagrangian particles:

$$r(t, r_0) = r(t, r_0 + \Delta) \quad \text{for } \Delta \neq 0.$$

Hence, taking into account the smallness of $\Delta \ll r_0$, we have

$$\begin{aligned} \Delta &= \frac{0.01\alpha^3}{N^{0.55}} \frac{r_0^2}{R_0(0)} \cos \left[\alpha \frac{r_0}{R_0(0)} \right] \cos \left[\alpha \frac{\Delta}{R_0(0)} \right] \\ &\times \ln \left[\frac{R_0(0) - U_0 t}{R_0(0)} \right]. \end{aligned}$$

It follows that, under the requirement $\Delta = \frac{R_0(0)}{10} \frac{r_0}{R_0(0)} \sim 0.5$, shock waves can only be formed under the unrealistic condition $\frac{R_0(0) - U_0 t}{R_0(0)} \sim 10^{-2}$. That is, during adiabatic compression of a relaxed system, shock waves are not formed.

Thus quantum shell effects in hydrodynamic processes manifest themselves only in the processes of system relaxation.

C. Numerical simulation results

In this subsection, we present results of numerical simulation that confirm the existence of a nonclassical mechanism of the compression of a submicron gas bubble. Suppose cold gas fills a spherical cavity, surrounded by a dense medium, e.g., diamond. The diamond is a good insulator, so its border acts as a quantum well potential with high amplitude. The effect described above emerges. When the system is compressed by external pressure, the effective force due to the quantum nature of the degenerate electronic component appends to gradients of pressure.

In simulations we consider the compression of hydrogen gas inside a cavity with $R = 1$ nm. The boundaries of the cavity converge toward the center with constant velocity. Initially gas has uniform density, $\rho = 5$ g/cm³, so the system is taken unrelaxed to a new external force. Initial temperature $T = 0.1$ eV. Simulations are carried out in a one-temperature single-fluid approximation (the dynamics of the ionic components is simulated explicitly). Details of the numerical code used are given in Appendix C and [26]. Such set-up

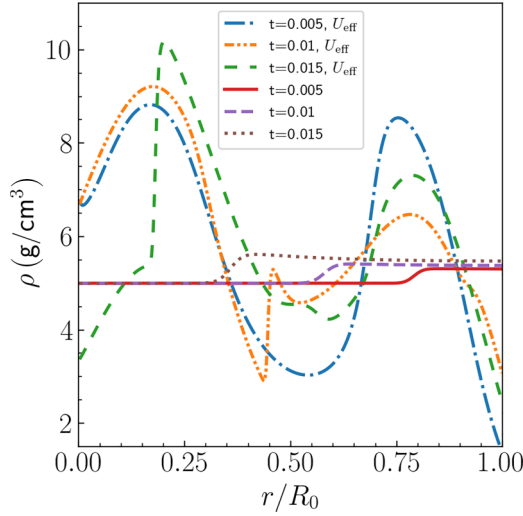


FIG. 1. Radial dependence of density (g/cm^3) for successive times $t = 0.005, 0.01, 0.015$ (early stage of compression) accounting for the U_{eff} and without the U_{eff} .

goals demonstrate the maximum possible impact by external force, which allows us to estimate the prospect of the effect.

Two calculations of submicron bubble compression are performed. The ionic system at the initial moment is taken to be unrelaxed in these calculations.

The first calculation is carried out with the effective potential $U_{\text{eff}}(r) = U_{\text{osc}}(r) + U_{\text{bar}}(r)$, where $U_{\text{osc}}(r)$ and $U_{\text{bar}}(r)$ are the oscillator and barrier potentials, which are modeled by the following expressions:

$$U_{\text{bar}} = -\frac{eV_0}{1 + \exp[(R_0 - r)/\delta]},$$

$$U_{\text{osc}} = C \left(\frac{\bar{n}}{10^{30}} \right)^{1/3} \frac{R_0(0)}{R_0(t)} f[r, R_0(t)].$$

In the second problem, we calculate the compression of the ion gas without taking into account the influence of the effective field ($U_{\text{eff}} = 0$). Comparison of the obtained results allows one to evaluate the magnitude of the effect.

The numerical calculations are carried out in dimensionless variables. The corresponding scales and transformation of the main hydrodynamic variables to the dimensionless form are described in Appendix C.

The following parameters are chosen for numerical calculations: the bubble radius is 1 nm; the gas density $\rho = 5 \text{ g}/\text{cm}^3$; the velocity at the outer boundary of the bubble $u_w = -2 \text{ km}/\text{s}$ is adopted; time interval $t_c = 0.45$, which corresponds to 90% gas compression; the barrier and oscillation potential parameters are fixed at the values $\delta = 0.1R_0$ and $C = 10 \text{ eV}$, $V_0 = 1 \text{ V}$.

The results of numerical simulation are shown in Figs. 1–4. Radial dependencies of density, velocity, pressure, and temperature are plotted for three successive time points corresponding to the initial stage of compression (about 3%).

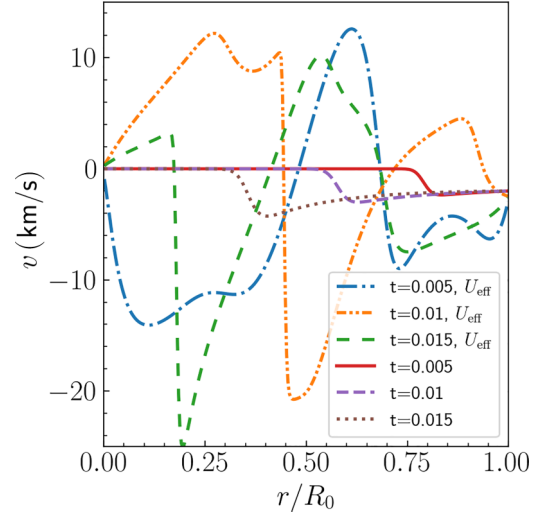


FIG. 2. Radial dependence of velocity (km/s) for successive times $t = 0.005, 0.01, 0.015$ (early stage of compression) with account for the U_{eff} and without the U_{eff} .

Let us compare the results of calculations without $U_{\text{eff}}(r)$ and with the presence of $U_{\text{eff}}(r)$. In the absence of $U_{\text{eff}}(r)$ compression evolves in accordance with the theory of classical gas dynamics, with the formation of a shock wave moving toward the center (shown by arrows in the figures). A qualitatively different picture arises if the effective potential is taken into account. The motion of the wall brings the system out of equilibrium, and the resulting field strongly affects the motion of the ions. A compression wave appears by the time $t = 0.005$, and the amplitude of the wave is several orders of magnitude higher than the amplitude of the shock in a purely gas-dynamic calculation. At subsequent moments, this wave overshoots forming a shock wave with the relative amplitude of about 1000. The velocity in the wave reaches the value of 20 km/s.

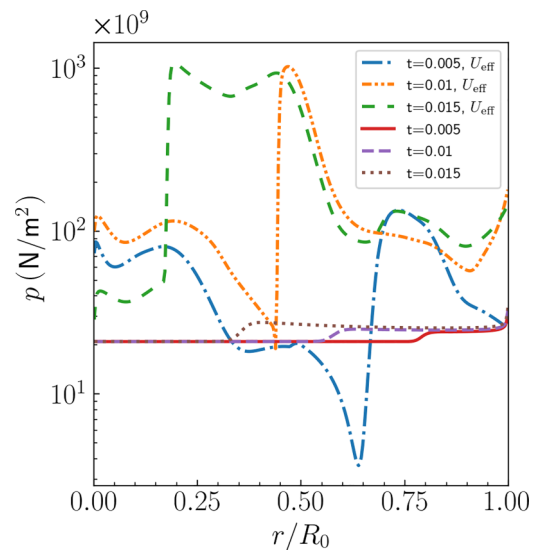


FIG. 3. Radial dependence of pressure for successive times $t = 0.005, 0.01, 0.015$ (early stage of compression) accounting for the U_{eff} and without the U_{eff} .

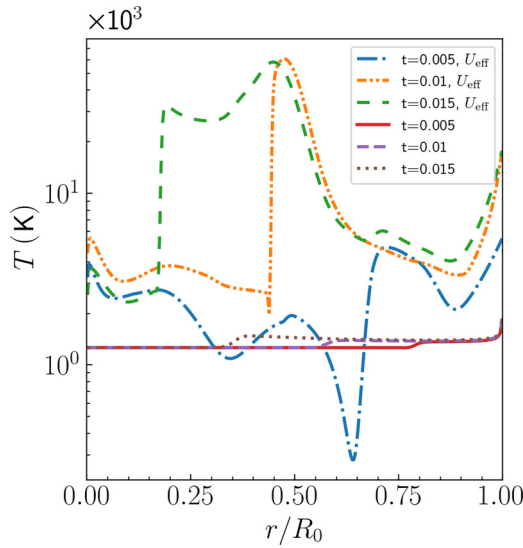


FIG. 4. Radial dependence of temperature (10^3 K) for successive times $t = 0.005, 0.01, 0.015$ (early stage of compression) accounting for the U_{eff} and without the U_{eff} .

Reaching the center, the wave causes a focusing of energy with a sharp rise in pressure and temperature in the center. This is seen in Figs. 5–7, which show the time dependence of the density, pressure, and temperature at the center of the spherical bubble.

Calculations without $U_{eff}(r)$ indicate the pressure increase by about two orders of magnitude when the shock wave focuses. Taking $U_{eff}(r)$ into account enhances this effect by almost 1000 times (Fig. 6). Similar effects emerge on the temperature graph. The temperature at the center increases by two orders of magnitude, reaching a value of ~ 1000 (10^3 K), at the moment of focusing of the shock wave which formed as a result of the compression wave overshooting due to the field.

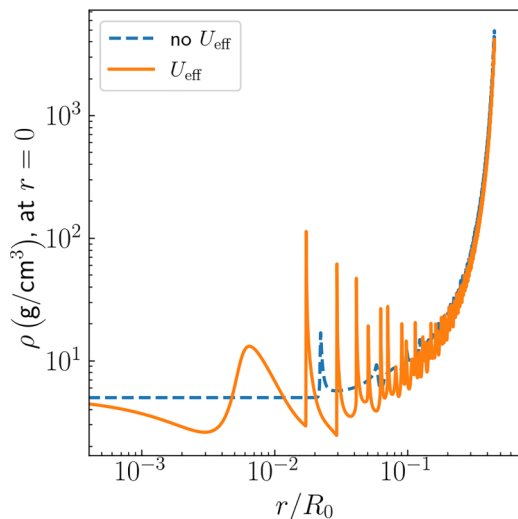


FIG. 5. Time dependence of density (g/cm^3) at the center of a spherical bubble accounting for the U_{eff} and without the U_{eff} .

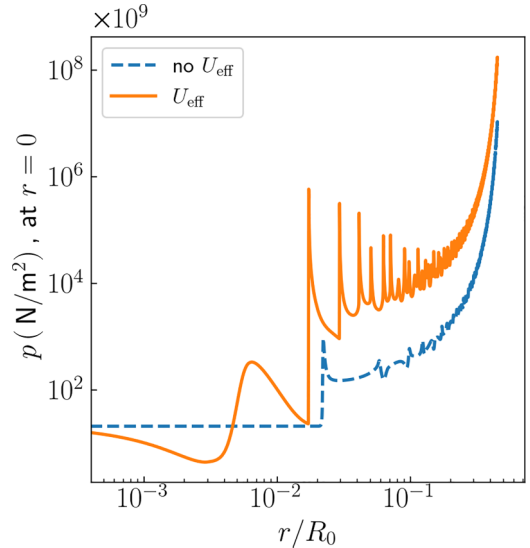


FIG. 6. Time dependence of pressure at the center of the spherical bubble accounting for the U_{eff} and without the U_{eff} .

The process of compression of the electron-ion system is accompanied by a series of multiple reflections of shock waves from the surface of the spherical bubble and subsequent focusing at the center.

This comparison of the results of calculations reveals that taking into account the quantum effect of a large spatial scale in the distribution of electrons qualitatively changes the nature of the cumulative processes.

Due to the large-scale electric field caused by quantum shell effects, the compression process is characterized by the formation of multiple shock waves. The values of gas temperature and pressure reached during compression turn out to be approximately two orders of magnitude higher as compared with the ordinary compression regime.

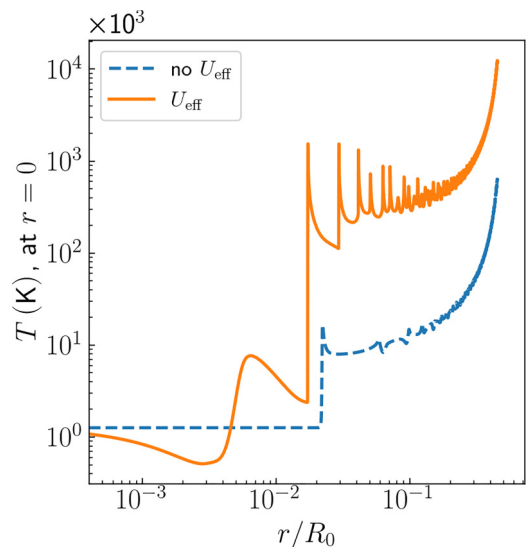


FIG. 7. Time dependence of temperature (10^3 K) at the center of the spherical bubble accounting for the U_{eff} and without the U_{eff} .

IV. CONCLUSION

A mechanism of hydrodynamic cumulation caused by quantum shell effects in a mesoscopic system consisting of a gas of degenerate electrons and a gas of classical ions has been identified and studied extensively.

The direct formulation, which implies self-consistent calculation of the gas-dynamic motion of ions and solving the quantum mechanical problem for determining the spatial distribution of the mesoscopic number of electrons, encounters significant computational complexity. Therefore, the simplified approach was elaborated upon. The main ingredients of such an approach are hydrodynamic description of the ionic and electronic subsystems and introduction of an external effective field acting on the electronic subsystem. This effective field allows one to take into account quantum effects in a simplified manner. The obtained results demonstrate validity and efficacy of the developed approach for the analysis of the considered class of problems.

The developed approach demonstrates that due to the presence of a large-scale electric field caused by quantum shell effects the process of gas bubble compression is accompanied by formation of the multiple shock waves. This drastically changes the character of the cumulative processes. The values of temperature and pressure in the central region increase by several orders of magnitude compared to the conventional compression regime.

The experimental study of the described effect is among the key future tasks. The temperature increasing in the bubble due to this effect could lead to the launching of thermonuclear reactions. Therefore, detection of fusion neutrons can be considered as strong evidence in favor of the effect discussed. The preliminary simplified calculations showed that cumulation in a nanoscale diamond target with a DT-ice central cavity could generate some neutrons. In this case, the energy spent on the generation of one neutron is comparable to the neutron energy cost in the record-breaking experiments at NIF [3]. In turn, the absence of the effect means the impossibility of ignition of thermonuclear fusion in such a system.

A difficult issue is the choice of a source for irradiating such a target. The direct laser irradiation requires the use of an extremely short wavelength laser due to the diffraction limit. On the other hand, the hohlraum experiment could break the implosion symmetry that is crucial for the effect considered. Moreover, the x-ray radiation could preheat the DT-ice cavity and hence violate the necessary conditions.

Nevertheless, the main problem of such an experiment is that a single target generates a number of neutrons that is well below the detectability threshold of the neutron detectors at currently operating laser facilities. The intuitive desire to increase the number of targets and place them into the hohlraum faces a number of serious technical problems. The fulfillment of the requirement of symmetry and synchronicity depends on how large the number of targets placed into the hohlraum is. It seems that a possible way to meet these requirements is to embed targets into a sub-critical-density plastic or carbon foam. It has been shown, however, both theoretically [27] and experimentally [28] that the laser generated heat front propagation velocity in such foams turns out to be microstructure dependent. Anyway the development of

the experiment idea is a nontrivial task and is beyond the scope of this paper. It could be the subject of a separate study.

ACKNOWLEDGMENT

The authors are grateful to Y. E. Lozovik for very helpful comments.

APPENDIX A: EFFECTIVE POTENTIAL

The effective potential is determined from the relation

$$\frac{1}{n_e^{\text{free}}} \frac{\partial p_e(n_e^{\text{free}})}{\partial r} = -e \frac{\partial}{\partial r} [U_{\text{eff}}(r)], \quad (\text{A1})$$

which is a consequence of the Euler equation of motion for the electron fluid and the spherical symmetry of the problem.

The electronic subsystem is considered within the Fermi gas model. Accordingly, the pressure and density of the electronic subsystem are related in the following way:

$$p_e = \frac{(3\pi^2)^{2/3}}{5} \left(\frac{\hbar^2}{m} \right) n_e^{5/3}. \quad (\text{A2})$$

In further calculations, it is convenient to use the dimensionless concentration \tilde{n}_e defined by the relation

$$\tilde{n}_e = 4\pi R_0^3 n_e, \quad (\text{A3})$$

$$\int_0^1 \tilde{n}_e \zeta^2 d\zeta = N_e, \quad (\text{A4})$$

where $\zeta = r/R_0$ is the dimensionless radial coordinate, and N_e is the number of electrons. The equation

$$\frac{(3\pi^2)^{2/3}}{2^{5/3}} \frac{\hbar^2}{mR_0^2} \frac{d\tilde{n}_e^{2/3}}{d\zeta} = \frac{dU_{\text{eff}}}{d\zeta} \quad (\text{A5})$$

follows directly from relations (A1)–(A4). This equation has the obvious solution

$$U_{\text{eff}} = \frac{(3\pi^2)^{2/3}}{2^{5/3}} \frac{\hbar^2}{mR_0^2} \tilde{n}_e^{2/3} + \text{const}. \quad (\text{A6})$$

Due to the smallness of the density fluctuations $\delta\tilde{n}_e$ as compared with the mean value \tilde{n}_e^0 , formula (A6) can be simplified:

$$\begin{aligned} U_{\text{eff}} &= \frac{(3\pi^2)^{2/3}}{2^{5/3}} \frac{\hbar^2}{mR_0^2} (\tilde{n}_e^0 + \delta\tilde{n}_e)^{2/3} \\ &\approx \frac{(3\pi^2)^{2/3}}{2^{5/3}} \frac{\hbar^2}{mR_0^2} \left[(\tilde{n}_e^0)^{2/3} + \frac{2}{3} \frac{\delta\tilde{n}_e}{(\tilde{n}_e^0)^{1/3}} \right]. \end{aligned} \quad (\text{A7})$$

Approximation (A7) loses its accuracy and becomes inapplicable near the wall ($r \sim R_0$, or $\zeta \sim 1$), which is due to vanishing of the electron density on the wall in accordance with the accepted boundary condition of the impenetrability of the wall in the quantum mechanical problem.

Figures 8–10 show examples of nonaveraged dependences $\tilde{u} = \tilde{n}_e^{2/3} - (\tilde{n}_e^0)^{2/3}$ for different values of the parameter $k_f R_0 \sim N^{1/3}$ ($k_f = p_f/\hbar$). The electron density is determined by means of direct summation over all the occupied states of electrons in the spherical potential well with infinite walls.

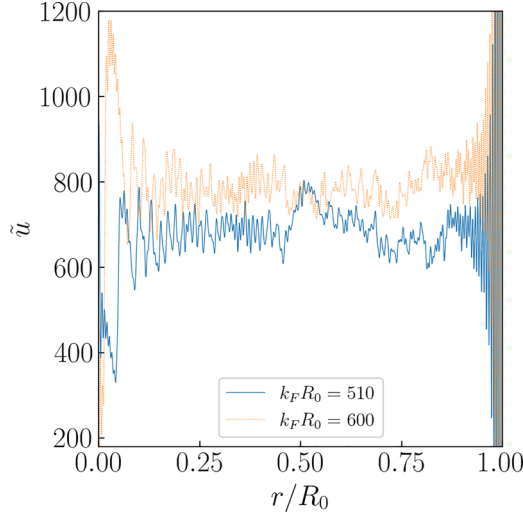


FIG. 8. Radial dependence of the effective potential for different values of $k_F R_0$.

Another technique based on the Green's function approach is also suitable for numerical calculation of the electron density. The method of constructing the Green's function based on two linearly independent solutions occurs rather conveniently for this purpose. As shown in Ref. [14] the results, obtained in these two ways, coincide with high accuracy. In itself the extent to which these results are consistent can be considered as an indicator of the accuracy of the numerical calculations.

With an appropriate choice of the constant in (A7), the quantity \tilde{u} is proportional to U_{eff} and can be considered as a dimensionless effective potential. Since the gas-dynamic calculation implies the use of averaged values over a large number of particles, the direct use of the value (A7) for such purposes is not correct. The density determined in the framework of quantum mechanics must be preliminarily averaged in a suitable way and only then should it be included in gas-dynamic calculations. The averaging procedure looks as

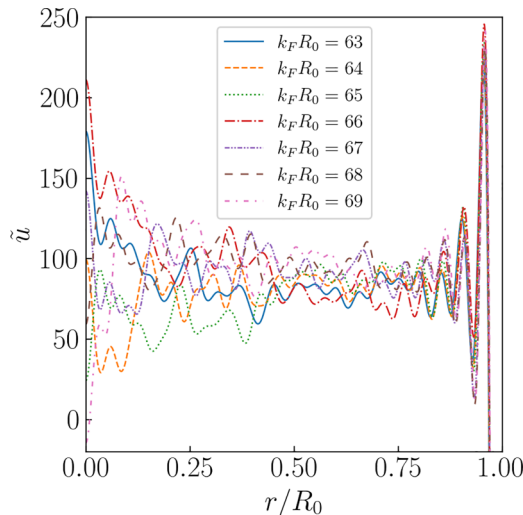


FIG. 9. Radial dependence of the effective potential for different values of $k_F R_0$.

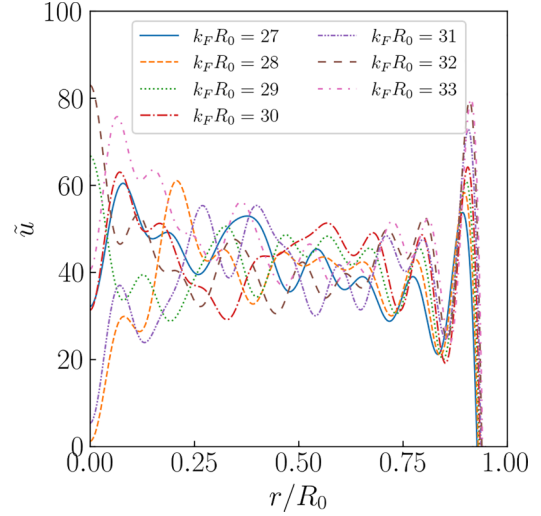


FIG. 10. Radial dependence of the effective potential for different values of $k_F R_0$.

follows. Due to spherical symmetry the averaging should be performed over a radial variable. For these purposes, we use averaging with the Gaussian weight function: $\exp[-\frac{(r-r')^2}{a^2}]$. The mean values of a certain quantity have the form

$$\bar{f}(r) = \frac{1}{C(r)} \int_0^{R_0} \exp[-(r-r')^2/a^2] f(r') dr', \quad (\text{A8})$$

where $\frac{1}{C(r)}$ is the normalization factor,

$$C(r) = \int_0^{R_0} \exp[-(r-r')^2/a^2] dr'.$$

Due to the finiteness averaging interval $[0, R_0]$ the factor $C(r)$ is coordinate dependent, which should be taken into account when calculating derivatives of $f(r)$.

Results of the averaging procedure (A8) with different values of the smearing parameter $a = 300h_r, 600h_r, 800h_r,$ and $1000h_r$ (h_r is the increment of uniform radial grid; the total number of grid nodes is equal to 10 000, correspondingly $h_r = R_0/10000$) are presented in Figs. 11–13. It can be seen that for $a = 1000h_r$, convergence in the averaged potential is achieved. This value of a was adopted below.

Figures 14–18 demonstrate the results of averaging of the function $\tilde{u} = \tilde{n}_e^{2/3} - (\tilde{n}_e^0)^{2/3}$ for $k_F R_0 \sim (28.0\text{--}33.0)$. This function differs from the effective potential by a constant factor only. The obtained results allow us to note the following patterns of behavior of U_{eff} . The shape of the effective potential depends on the number of particles and has from one to three bumps. There is some periodicity of the potential shape (see Fig. 18) when changing the number of particles. The characteristic period is approximately equal to $\Delta k_F R_0 \sim (1.3\text{--}1.4)$ in this dependence. The amplitude of the effective potential U_{eff} is proportional to $\frac{1}{R_0^3}$ and weakly depends on N . The behavior is similar for other values of $k_F R_0$ (see Fig. 19).

The electrostatic potential of the electronic subsystem is calculated in the usual way:

$$U_c = \int_V \frac{e}{4\pi\epsilon_0} \frac{1}{|r-r'|} n_e(r') d^3 r'. \quad (\text{A9})$$

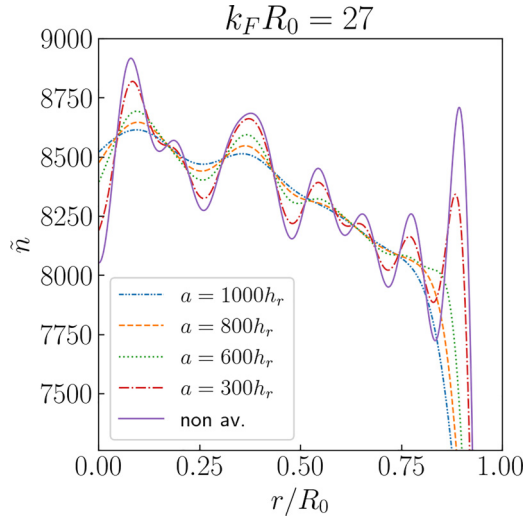


FIG. 11. Radial dependence of the electron density and averaged ones obtained with different values of the smearing parameter; $k_F R_0 = 27$.

Spherical symmetry simplifies Eq. (A9):

$$U_c = \frac{e}{4\pi\epsilon_0 R_0} \left\{ \frac{1}{\zeta} \int_0^\zeta \tilde{n}_e(\zeta') \zeta'^2 d\zeta' + \int_\zeta^1 \tilde{n}_e(\zeta') \zeta' d\zeta' \right\}. \quad (\text{A10})$$

The first term in Eq. (A10) is the potential on the surface of the ball of radius r and the second one is the potential of a spherical layer on its inner boundary.

We also calculate large-scale spatial oscillations $\varphi_{\text{electr}}^{\text{free}}$ — the electric potential of an electrically neutral system consisting of noninteracting electrons and a spatially homogeneous ball of ions. This value allows one to estimate the shape and magnitude of the electric force acting on the ionic system.

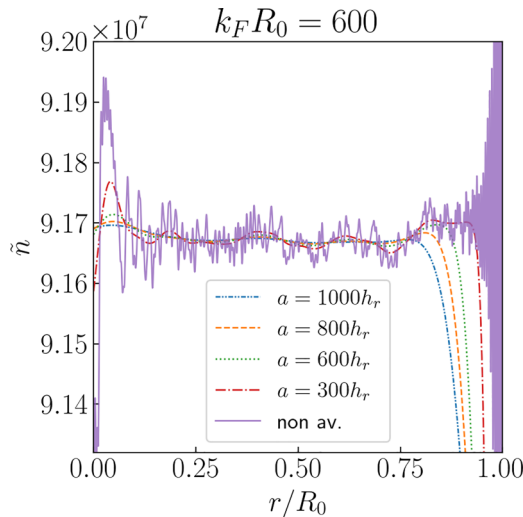


FIG. 12. Radial dependence of the electron density and averaged ones obtained with different values of the smearing parameter; $k_F R_0 = 600$.

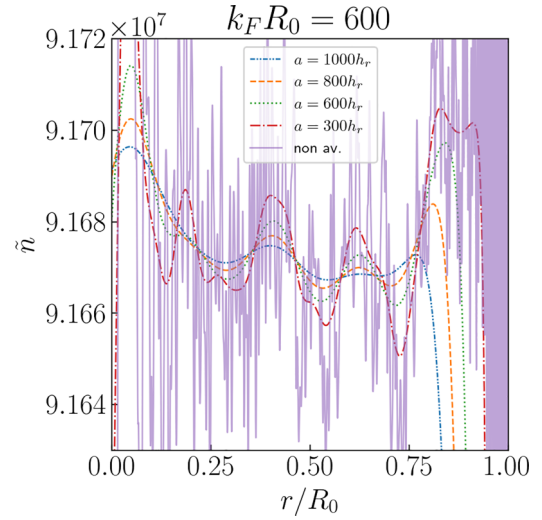


FIG. 13. The same as in Fig. 12, but with an enlarged scale along the vertical axis.

It should be emphasized that the electrostatic potential defined by Eqs. (A9) and (A10) is not directly connected with effective potential (A1).

The potential (A10) should be supplemented with the potential created by ions. Within the approximate model, a homogeneous ion background is considered, and accordingly its potential is that of a uniformly charged ball. In this case, the following circumstance should be taken into account. The zero boundary condition on the wall of the cavity in the quantum mechanical problem causes vanishing of the electron density on the wall. This circumstance should be taken into account in the model ionic density. Namely, the ionic density is modeled by a uniformly charged ball with a slightly smaller radius than R_0 . The reference point for choosing the ion distribution radius is zeroing of the total potential of electrons and ions on the wall (i.e., at $r = R_0$).

Averaging, similar to that applied to U_{eff} , should also be applied to U_c . It should be noted that the radial dependence of the unaveraged potential U_c differs significantly from U_{eff} . This is due to U_{eff} being proportional to $\tilde{n}_e^{2/3}$, which is a rapidly oscillating function, while U_c is defined through integration of \tilde{n}_e in (A10). Integration smears out these high-frequency oscillations. Nevertheless, the uniformity of the approach implies that averaging should be applied to U_c also.

Figures 20–22 show the results of averaging the electric potentials $\varphi_{\text{electr}}^{\text{free}}$ (made dimensionless by the parameter $\frac{e}{4\pi\epsilon_0} \frac{1}{R_0}$) for different values of the parameters $k_F R_0 \sim N^{1/3}$. It can be seen from Figs. 20–22 that the behavior of the potential $\varphi_{\text{electr}}^{\text{free}}$ is in qualitative accordance with the shape of the potential U_{eff} .

Based on the calculated values U_c the electron densities for the systems with $k_F R_0 = 27600$ are computed by means of the Poisson equation. These results are presented in Figs. 23 and 24.

The closeness of the results confirms the similarity of the two methods of averaging.

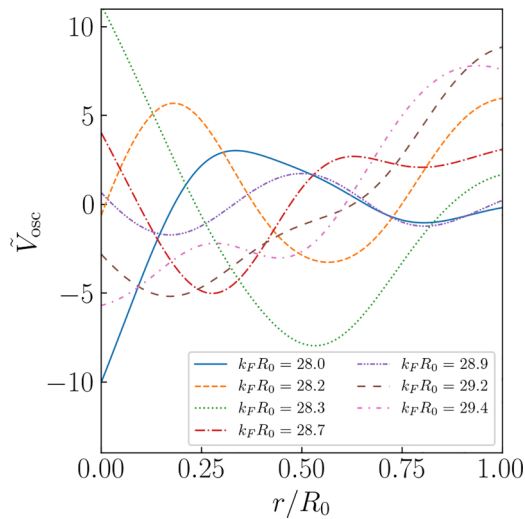


FIG. 14. Radial dependence of the oscillation potential for several values of $k_F R_0$.

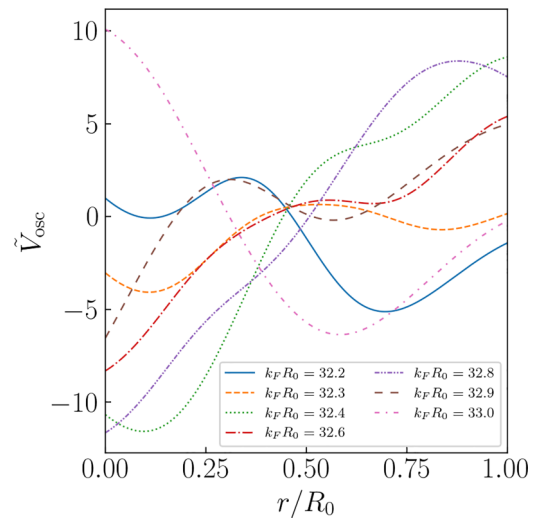


FIG. 17. Radial dependence of the oscillation potential for several values of $k_F R_0$.

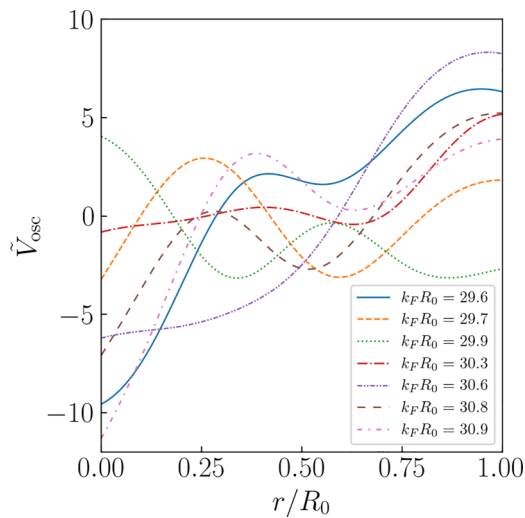


FIG. 15. Radial dependence of the oscillation potential for several values of $k_F R_0$.

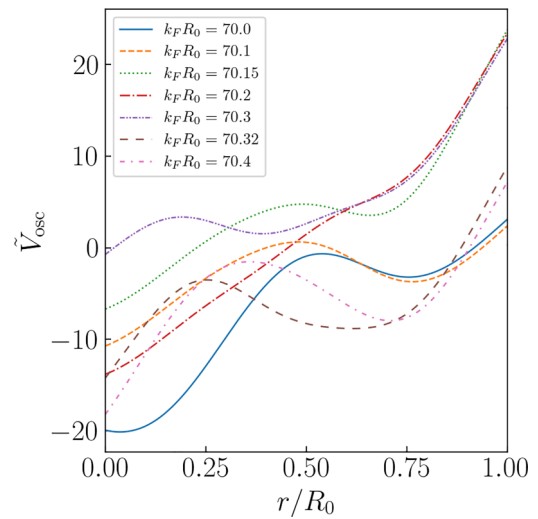


FIG. 18. Radial dependence of the oscillation potential for several values of $k_F R_0$.

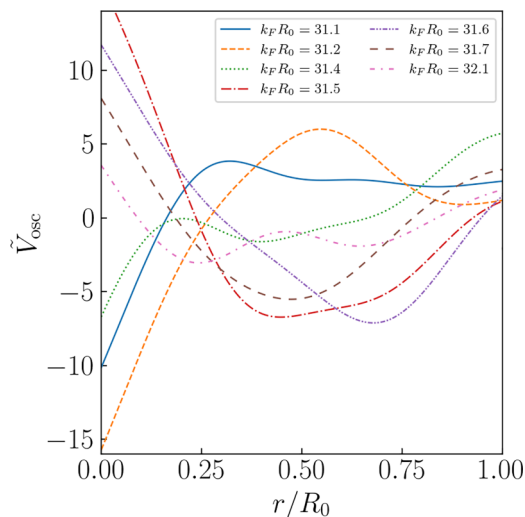


FIG. 16. Radial dependence of the oscillation potential for several values of $k_F R_0$.

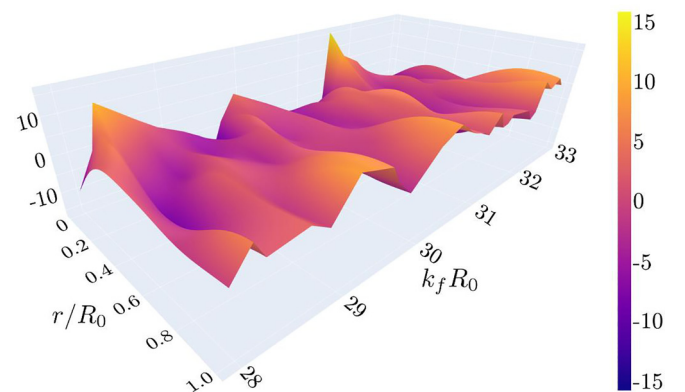


FIG. 19. 3D plot of the dimensionless effective potential as a function of the radial coordinate and the parameter ($k_F R_0$). Quasiperiodicity appears in the ($k_F R_0$) dependence.

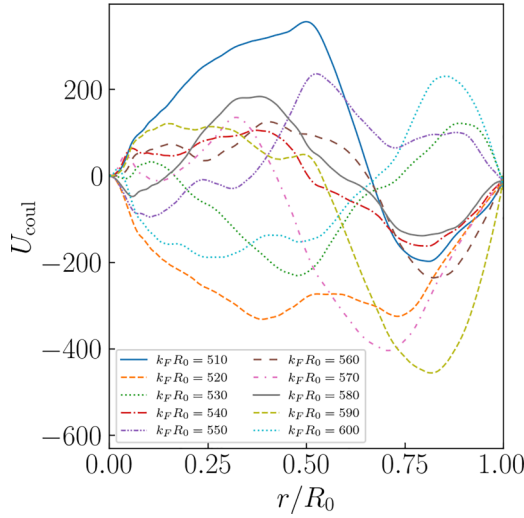


FIG. 20. Radial dependence of the Coulomb potential for several values of $k_F R_0$.

APPENDIX B: MODEL APPROXIMATION OF THE EFFECTIVE POTENTIAL

A characteristic feature of the effective potential U_{eff} is its fluctuating behavior near the mean value, and a sharp drop to zero at the cavity boundary. To convey the abrupt behavior in the near-wall region, the Woods-Saxon function for the barrier potential can be used:

$$f_{\text{ws}}(r) = \frac{W}{1 + \exp[(r - R_{\text{ws}})/a]},$$

where R_{ws} is the distribution radius, a is diffuseness, and the parameter W determines the average value inside the cavity. By varying these three parameters, we achieve the best reproduction of U_{eff} , by means of minimizing the sum of squared deviations of U_{eff} values on the grid from the approximant

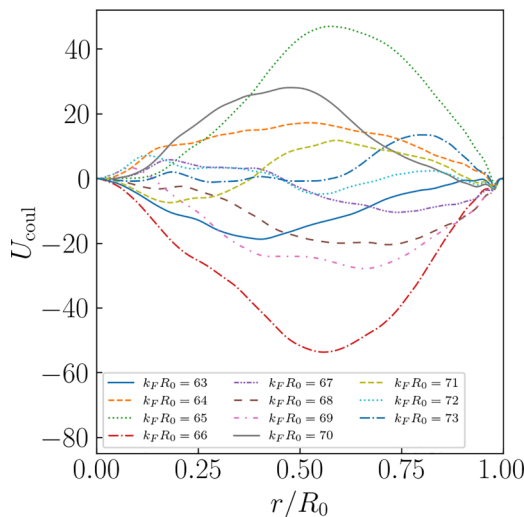


FIG. 21. Radial dependence of the Coulomb potential for several values of $k_F R_0$.

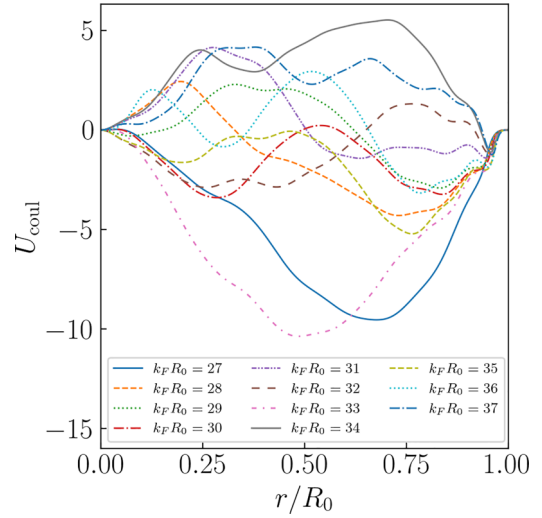


FIG. 22. Radial dependence of the Coulomb potential for several values of $k_F R_0$.

f_{ws} . That is we are looking for:

$$\min \left(\sum_{i=1}^N [U_{\text{eff}}(r_i) - f_{\text{ws}}(r_i)]^2 \right),$$

on the grid $\{r_i\}_{i=1}^N$. This part of the effective potential is referred to as the barrier potential. The next step in the approximation is to take into account oscillations of U_{eff} near the mean value inside the cavity. Bearing in mind the use of this potential in the gas-dynamic calculation, it should, as noted above, be averaged over high-frequency oscillations in order to reveal large-scale dependencies. Thus the approximant should reproduce not high-frequency fluctuations, but rather a smoothed behavior. To do this, a rapidly changing quantity $[U_{\text{eff}}(r_i) - f_{\text{ws}}(r_i)]$ was preliminarily averaged with

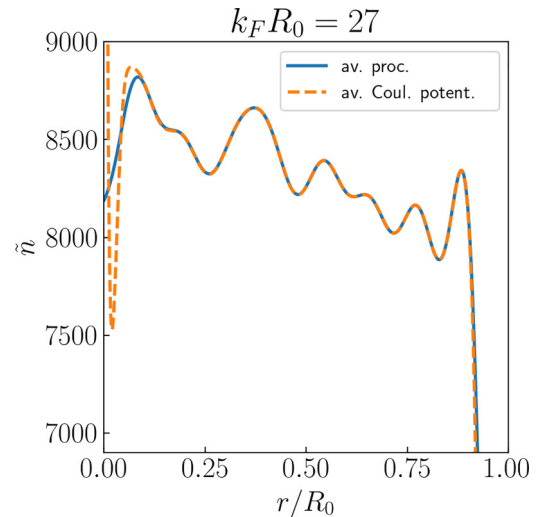


FIG. 23. Radial dependence of the electron density obtained by means of the averaging procedure (A8) and that from the averaged Coulomb potential; $k_F R_0 = 27$.

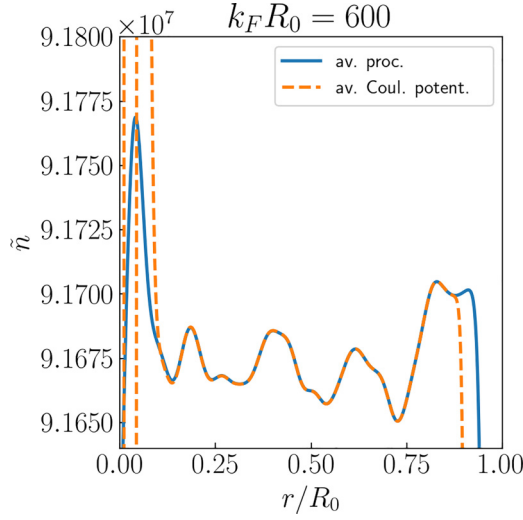


FIG. 24. Radial dependence of the electron density obtained by means of the averaging procedure (A8) and that from the averaged Coulomb potential; $k_F R_0 = 600$.

a Gaussoid (see (A8)). The averaged values obtained in this way for the quantity $[U_{\text{eff}}(r_i) - f_{\text{WS}}(r_i)]$ are much smoother, and the characteristic spatial scale of their change is comparable to the size of the cavity. It is convenient to approximate

this dependence by a partial sum of the Fourier series with the retention of five to ten terms depending on the desired accuracy:

$$\overline{[U_{\text{eff}}(r_i) - f_{\text{WS}}(r_i)]} \approx \sum_{m=0}^M C_m \cos\left(\pi m \frac{r}{R_0}\right).$$

This part of the effective potential is referred to as the oscillation part. It should be noted that averaging and representation by a partial sum of the Fourier series should be carried out only after separation of the barrier potential. The point is that the origin of the barrier potential is related to the boundary condition, which is rather rigid (vanishing of the wave functions on the cavity wall) and is not the effect of the appearance of a large scale in the oscillating part of U_{eff} .

Table I shows the values of the coefficients \tilde{C}_m that differ from the Fourier coefficients in the above formula by a constant factor $C_m = \frac{(3p)^{2/3}}{2^{5/3}} \frac{\hbar^2}{mR_0^2} \tilde{C}_m$. The choice of parameter values $k_F R_0$ corresponds to the dependencies shown in Figs. 14–17.

As calculations demonstrate it is sufficient to keep the first few terms of the Fourier series to provide a good approximation and the use of a partial sum which includes the first five to six terms is sufficient in most cases (see Figs. 25–29).

TABLE I. Expansion coefficients of the Fourier series of the oscillation potential for several values of $k_F R_0$.

$k_F R_0$	\tilde{C}_0	\tilde{C}_1	\tilde{C}_2	\tilde{C}_3	\tilde{C}_4	\tilde{C}_5
28.0	-0.3894	-0.7383	-2.8435	-2.3562	-0.9652	-0.8250
28.2	2.9122	0.6681	3.6358	-2.1092	-1.0644	-0.8042
28.3	-3.1570	2.9068	6.5422	0.7503	0.4930	0.4791
28.7	0.4062	-2.6594	0.8154	2.3031	1.6555	0.2033
28.9	-0.3627	-0.1521	-1.0935	-0.0176	0.9988	0.1052
29.2	-0.3176	-5.7909	1.7601	-0.7042	0.8527	0.3029
29.4	0.6283	-5.9594	1.9040	-0.7174	-1.0703	-0.0243
29.6	1.7177	-5.9279	-1.5893	-2.1648	-0.6561	0.2338
29.7	-0.0855	0.4883	1.0883	-2.2426	-1.0793	-0.2200
29.9	-2.4844	1.7689	0.7406	1.7640	1.0054	-0.2371
30.3	1.5828	-1.7354	1.0854	-1.1616	0.4130	0.0061
30.6	-0.6460	-7.3809	1.8339	0.0736	-0.3225	0.1087
30.8	-0.4265	-3.4219	1.1895	-1.9458	-1.3187	-0.2825
30.9	0.1190	-3.8300	-2.3894	-3.1061	-0.7394	-0.0401
31.1	2.7634	-2.1295	-2.5225	-2.1742	-1.4719	-0.8770
31.2	0.7209	-4.6133	-5.7273	-1.6699	-0.6225	-0.9914
31.4	0.2390	-2.9134	1.1446	-1.2851	-0.4283	-0.9020
31.5	-2.3328	4.4380	6.9176	2.0165	1.6176	0.1689
31.6	-2.1147	5.0537	4.7025	-0.4851	1.6173	0.1854
31.7	-1.8350	0.2293	4.9661	1.0755	0.6322	0.4484
32.1	-1.7792	-0.5736	1.3271	0.1972	1.3385	0.6589
32.2	-2.7766	2.7040	0.0689	-2.0208	0.4551	0.3902
32.3	-2.0369	-1.6110	-1.4754	-0.2839	0.4066	0.1129
32.4	-1.6902	-9.7029	-1.7350	-0.3147	1.1100	0.1335
32.6	-0.9042	-4.4818	-0.9866	-1.6367	0.1355	-0.4134
32.8	-0.1031	-9.3432	-0.5977	-0.1401	-0.8784	-0.1079
32.9	1.7022	-2.4418	-0.0656	-2.1678	-0.9110	-0.3942
33.0	-1.6393	5.0189	5.0646	0.1092	0.2522	0.0300

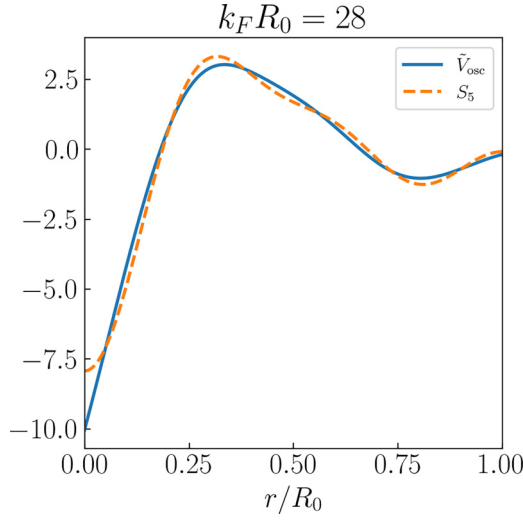


FIG. 25. Radial dependencies of the averaged oscillation potential and its Fourier series partial sum; $k_F R_0 = 28$.

Table II shows the values of the coefficients for the barrier potential. The choice of the values of parameter $k_F R_0$ corresponds to the graphics in Figs. 14–17.

APPENDIX C: NUMERICAL ALGORITHM

We consider the sphere of the initial radius R_0 consisting of a gas of degenerate electrons with density $n_e(r, t)$ and classical ions with density n_i . It is assumed that the electron density satisfies the equilibrium condition at each time moment:

$$-e \frac{\partial}{\partial r} (\varphi + U_{\text{osc}} - U_{\text{bar}}) + \frac{1}{n_e} \frac{\partial p_e}{\partial r} = 0, \quad (\text{C1})$$

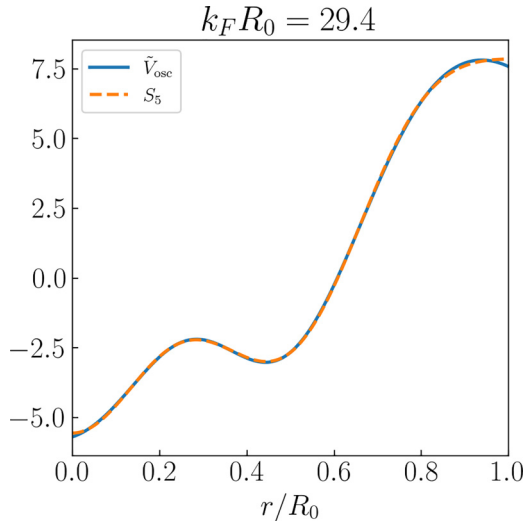


FIG. 26. Radial dependencies of the averaged oscillation potential and its Fourier series partial sum; $k_F R_0 = 29.4$.

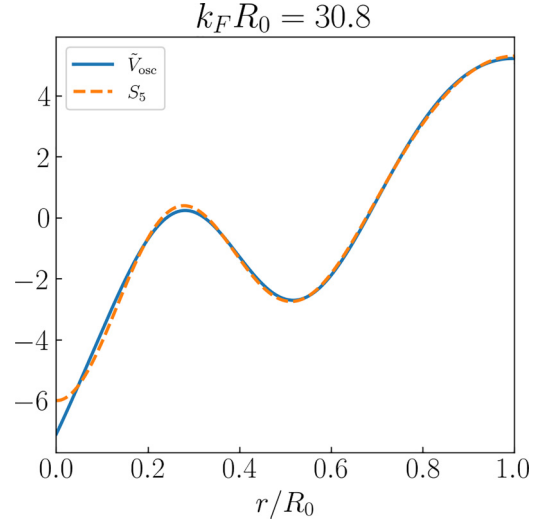


FIG. 27. Radial dependencies of the averaged oscillation potential and its Fourier series partial sum; $k_F R_0 = 30.8$.

where U_{osc} and U_{bar} are the oscillating and barrier potentials, respectively:

$$U_{\text{osc}}(r) = \sum_m^M C_m \cos\left(\pi m \frac{r}{R_0}\right),$$

$$U_{\text{bar}}(r) = \frac{W}{1 + \exp\left(\frac{r - R_{\text{ws}}}{a}\right)}, \quad (\text{C2})$$

where C and W are the characteristic amplitudes of the oscillating and barrier potentials, and a is the size of the barrier potential.

The electron pressure depends on the local electron density and is determined by the following expression:

$$p_e = \frac{(3\pi^2)^{2/3} \hbar^2}{5 m_e} (n_e)^{5/3}. \quad (\text{C3})$$

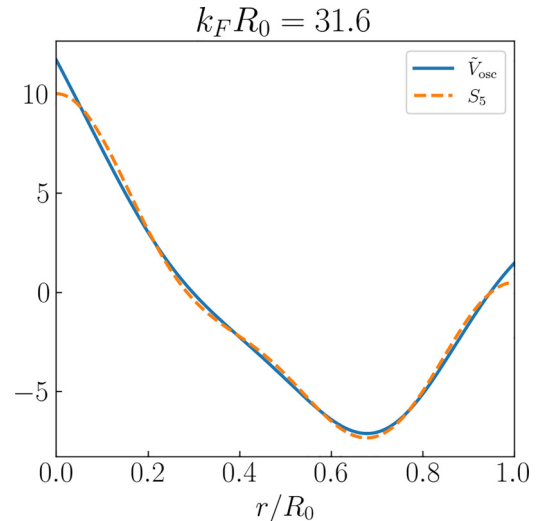


FIG. 28. Radial dependencies of the averaged oscillation potential and its Fourier series partial sum; $k_F R_0 = 31.6$.

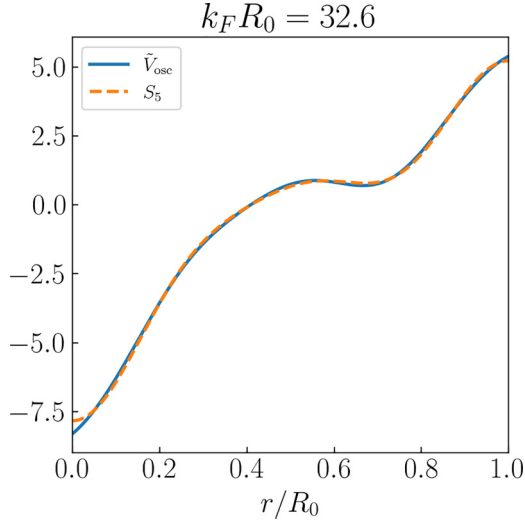


FIG. 29. $k_F R_0 = 32.6$ Radial dependencies of the averaged oscillation potential and its Fourier series partial sum.

The motion of the ion gas is a result of the action on the ions from the electrostatic field created by the instantaneous distribution of ions and electrons. The ion gas is assumed to be ideal, i.e., the effects of viscosity and thermal conductivity are neglected, and is calorically perfect with the equation of state $p = (\gamma - 1)\rho\zeta$, where $\gamma = 5/3$ is the adiabatic exponent, p is the pressure, and ζ is the specific internal energy.

It can be shown that the influence of nonequilibrium between the distribution of ions and electrons takes place in a very small neighborhood of the wall. Therefore, in the gas-dynamics calculations described below, it is assumed that there is a local equilibrium at all points inside the sphere $n_i = n_e$. Then the electron pressure determines the ion distribution.

The medium inside the sphere is assumed to be electroneutral, therefore at each moment the distributions of electrons and ions satisfy the condition of zero total charge:

$$\int_0^{R_0(t)} n_e(r, t) r^2 dr = \int_0^{R_0(t)} n_i(r, t) r^2 dr, \quad n_i = \rho/m_i,$$

where m_i is the mass of ions.

The ion motion is described by the standard system of Euler equations for gas dynamics under the assumption of spherical symmetry. This system is supplemented by the right-hand side corresponding to the change in momentum and energy due to the electrostatic field produced by charged particles in the gas (ions and free electrons):

$$\begin{aligned} \frac{\partial \rho}{\partial t} + \frac{\partial(\rho U)}{\partial r} &= -\frac{2}{r} \rho U, \\ \frac{\partial(\rho U)}{\partial t} + \frac{\partial(\rho U^2 + p)}{\partial r} &= -\frac{2}{r} \rho U^2 - \frac{e}{m_i} \rho \frac{\partial \varphi}{\partial r}, \\ \frac{\partial(\rho E)}{\partial t} + \frac{\partial(\rho UH)}{\partial r} &= -\frac{2}{r} \rho UH - \frac{e}{m_i} \rho U \frac{\partial \varphi}{\partial r}, \end{aligned} \quad (\text{C4})$$

where e is the electron charge, $E = 0.5 U^2 + \zeta$ is the specific total ion energy, $H = \zeta + p/\rho$ is the specific total enthalpy, $\zeta = p/\rho/(\gamma-1)$ is the specific internal energy of the ions,

TABLE II. Parameters of the barrier potential for several values of $k_F R_0$.

$k_F R_0$	$R_{WS}/R_0, 10^{-1}$	$a/R_0, 10^{-2}$	W
28.0	9.62	1.35	439.6
28.2	9.63	1.28	447.0
28.3	9.63	1.30	463.9
28.7	9.63	1.29	471.2
28.9	9.63	1.31	476.8
29.2	9.64	1.22	480.3
29.4	9.65	1.21	489.2
29.6	9.65	1.22	493.5
29.7	9.65	1.24	499.9
29.9	9.65	1.26	515.4
30.3	9.66	1.19	521.8
30.6	9.66	1.16	527.2
30.8	9.66	1.18	532.5
30.9	9.66	1.19	537.0
31.1	9.66	1.20	545.7
31.2	9.66	1.20	551.3
31.4	9.67	1.15	560.3
31.5	9.67	1.17	566.2
31.6	9.66	1.18	571.6
31.7	9.67	1.15	575.2
32.1	9.67	1.16	579.9
32.2	9.67	1.18	585.7
32.3	9.67	1.17	589.8
32.4	9.68	1.10	597.5
32.6	9.68	1.11	602.5
32.8	9.69	1.09	605.9
32.9	9.68	1.11	615.9
33.0	9.68	1.14	622.7

$\gamma = 5/3$, and $0 \leq r \leq R(t)$. The potential is determined by the Eq. (C1), where we use n_e instead of n_i .

We rewrite the system of Eqs. (C1) and (C4) in dimensionless form. To do this, we introduce the scales of the characteristic physical quantities in the following form:

$$\begin{aligned} \rho_* &= 10^3 \text{ kg/m}^3: \text{ density;} \\ L_* &= 10^{-6} \text{ m: length;} \\ U_* &= 10^3 \text{ m/s: velocity;} \\ t_* &= L_*/U_* = 10^{-9} \text{ s: time;} \\ p_* &= \rho_* U_*^2 = 10^9 \text{ N/m}^2: \text{ pressure;} \\ \varphi_* &= m_i U_*^2/eV = 1.875 \times 10^{-2} \text{ V: potential of electric field;} \\ \Theta_* &= m_i U_*/et_* = 1.875 \times 10^4 \text{ V/m: electric field.} \end{aligned}$$

The values of the physical parameters of the model are as follows:

$$\begin{aligned} e &= 1.6 \times 10^{-19} \text{ Cl: electron charge;} \\ m_i &= 3 \times 10^{-27} \text{ kg: ion mass.} \end{aligned}$$

The system of Eqs. (C4) can be written in a conservative form. In dimensionless variables, it has the following form:

$$\begin{aligned} \frac{\partial r^2 \rho}{\partial t} + \frac{\partial(r^2 \rho U)}{\partial r} &= 0, \\ \frac{\partial(r^2 \rho U)}{\partial t} + \frac{\partial r^2(\rho U^2 + p)}{\partial r} &= 2rp - \rho r^2 \frac{\partial \varphi}{\partial r}, \\ \frac{\partial r^2(\rho E)}{\partial t} + \frac{\partial r^2(\rho UH)}{\partial r} &= \rho U r^2 \frac{\partial \varphi}{\partial r}, \end{aligned} \quad (\text{C5})$$

where the gradient of the potential

$$\frac{\partial \varphi}{\partial r} = K_1 \rho^{-1/3} \frac{\partial \rho}{\partial r} + K_3 \left[\frac{R_0(0)}{R_0(t)} \right]^2 \frac{\partial U_{\text{bar}}}{\partial r} - K_4 \frac{R_0(0)}{R_0(t)} \frac{\partial f(r, R_0(t))}{\partial r}.$$

The dimensionless constants are as follows:

$$\begin{aligned} K_1 &= \frac{(3\pi^2)^{2/3}}{3} \frac{\hbar^2}{em_e \varphi_*} (n_*)^{2/3}, \quad n_* = \rho_*/m_i \\ K_3 &= \frac{\hbar^2}{2em_e \varphi_*} \left(3\pi^2 \frac{\rho_0}{m_i} \right)^{2/3} \left[\frac{R_0(0)}{R_0(t)} \right]^2, \\ K_4 &= C \frac{10^{-10} m}{\varphi_*} \left(\frac{\rho_0}{m_i} \right)^{1/3}. \end{aligned}$$

If we introduce the total pressure,

$$\pi = p + \frac{3}{5} K_1 (\rho)^{5/3},$$

the system of Eqs. (C5) can be rewritten as follows:

$$\begin{aligned} \frac{\partial r^2 \rho}{\partial t} + \frac{\partial (r^2 \rho U)}{\partial r} &= 0, \\ \frac{\partial (r^2 \rho U)}{\partial t} + \frac{\partial r^2 (\rho U^2 + \pi)}{\partial r} - 2r\pi &= \rho r^2 \left\{ K_3 \left[\frac{R_0(0)}{R_0(t)} \right]^2 \frac{\partial U_{\text{bar}}}{\partial r} - K_4 \frac{R_0(0)}{R_0(t)} \frac{\partial f[r, R_0(t)]}{\partial r} \right\}, \\ \frac{\partial r^2 (\rho E)}{\partial t} + \frac{\partial r^2 \rho U (E + \pi/\rho)}{\partial r} &= \frac{3}{5} K_1 (\rho)^{5/3} \frac{\partial r^2 u}{\partial r} - \rho r^2 U \left\{ K_3 \left[\frac{R_0(0)}{R_0(t)} \right]^2 \frac{\partial U_{\text{bar}}}{\partial r} - K_4 \frac{R_0(0)}{R_0(t)} \frac{\partial f[r, R_0(t)]}{\partial r} \right\}, \end{aligned} \quad (\text{C6})$$

Except for the right-hand side, the system of Eqs. (C6) coincides exactly with the classical system of equations of gas dynamics with the equation of state (EOS) in the following form:

$$\pi = (\gamma - 1) \rho e + \frac{3}{5} K_1 (\rho)^{5/3}. \quad (\text{C7})$$

The numerical integration of (C6) can be performed by the Godunov method,

$$\mathbf{q}_i^{n+1} = \frac{3}{(r_{i+1/2}^{n+1})^3 - (r_{i-1/2}^{n+1})^3} \left\{ \frac{(r_{i+1/2}^n)^3 - (r_{i-1/2}^n)^3}{3} \mathbf{q}_i^n - \Delta t \left[(r_{i+1/2}^{n+1/2})^2 \mathbf{F}_{i+1/2} - (r_{i-1/2}^{n+1/2})^2 \mathbf{F}_{i-1/2} + \mathbf{S}_{\pi,i} + \mathbf{S}_{U,i} \right] \right\}.$$

Here F denotes the fluxes in divergence terms of the system (C6), and

$$\begin{aligned} \mathbf{S}_{\pi,i} &= \begin{bmatrix} 0 \\ \left[(r_{i+1/2}^{n+1/2})^2 - (r_{i-1/2}^{n+1/2})^2 \right] \pi_i \\ 0 \end{bmatrix}, \\ \mathbf{S}_{U,i} &= \begin{bmatrix} 0 \\ \left[(r_{i+1/2}^{n+1/2})^3 - (r_{i-1/2}^{n+1/2})^3 \right] \rho_i S_{2,i} \\ \left[(r_{i+1/2}^{n+1/2})^2 U_{i+1/2} - (r_{i-1/2}^{n+1/2})^2 U_{i-1/2} \right] 3K_1 (\rho_i)^{5/3} / 5 + \left[(r_{i+1/2}^{n+1/2})^3 - (r_{i-1/2}^{n+1/2})^3 \right] \rho_i U_i S_{3,i} \end{bmatrix}. \end{aligned} \quad (\text{C8})$$

Here, the right-hand side of the equations is related with the barrier and oscillating potential, and the values at the edges of the cells (half-integral indices) are determined from the solution of the Riemann problem. To solve the Riemann problem, we use the local approximation of the EOS (C7),

$$\pi = (\gamma - 1) \rho e + c_0^2 (\rho - \rho_0), \quad (\text{C9})$$

where the parameters of the EOS are approximated from the value of the local density by the following relations:

$$\rho_0 = \frac{2}{3} \rho, \quad c_0^2 = K_1 \rho^{2/3}. \quad (\text{C10})$$

The Courant number is determined by the speed of sound of the system (C6) to provide stability of the numerical scheme.

$$c^2 = \frac{\gamma(\pi + \pi_0) \rho e + \frac{3}{5} K_1 (\rho)^{5/3}}{\rho}, \quad \pi_0 = \frac{2}{5\gamma} K_1 (\rho)^{5/3}. \quad (\text{C11})$$

- [1] J. Lindl, O. Landen, J. Edwards, E. Moses, and N. Team, Review of the national ignition campaign 2009–2012, *Phys. Plasmas* **21**, 020501 (2014).
- [2] E. I. Moses, J. D. Lindl, M. L. Spaeth, R. W. Patterson, R. H. Sawicki, L. J. Atherton, P. A. Baisden, L. J. Lagin, D. W. Larson, B. J. MacGowan *et al.*, Overview: Development of the national ignition facility and the transition to a user facility for the ignition campaign and high energy density scientific research, *Fusion Sci. Technol.* **69**, 1 (2016).
- [3] A. B. Zylstra, A. L. Kritcher, O. A. Hurricane, D. A. Callahan, K. Baker, T. Braun, D. T. Casey, D. Clark, K. Clark, T. Doppner *et al.*, Record energetics for an inertial fusion implosion at NIF, *Phys. Rev. Lett.* **126**, 025001 (2021).
- [4] N. Fleurot, C. Cavailler, and J. Bourgade, The Laser Mega-joule (LMJ) Project dedicated to inertial confinement fusion: Development and construction status, *Fusion Eng. Des.* **74**, 147 (2005).
- [5] S. Bel'kov, S. Garanin, and Y. Shagalkin, The UFL-2M facility: First steps on the way to its construction, in *Book of Abstracts of the XL International Zvenigorod Conference on Plasma Physics and Controlled Fusion* (ZAO NTTs PLAZMAIOFAN, Moscow, 2013).
- [6] V. B. Rozanov, S. Y. Gus'kov, G. A. Vergunova, N. N. Demchenko, R. V. Stepanov, I. Y. Doskoch, R. A. Yakhin, and N. V. Zmitrenko, Direct drive targets for the megajoule facility UFL-2M, *J. Phys.: Conf. Ser.* **688**, 012095 (2016).
- [7] T. W. L. Sanford, R. E. Olson, R. L. Bowers, A. Chandler, M. S. Derzon, D. E. Hebron, R. J. Leeper, R. C. Mock, T. J. Nash, D. L. Peterson *et al.*, Z-pinch-generated x rays demonstrate potential for indirect-drive ICF experiments, *Phys. Rev. Lett.* **83**, 5511 (1999).
- [8] J. Meyer-ter-Vehn, Fast ignition of ICF targets: An overview, *Plasma Phys. Controlled Fusion* **43**, A113 (2001).
- [9] S. Garanin, A. Ivanovsky, and L. Mkhitarian, An ICF system based on Z-pinch radiation produced by an explosive magnetic generator, *Nucl. Fusion* **51**, 103010 (2011).
- [10] S. J. Putterman, *Superfluid Hydrodynamics* (North-Holland, Amsterdam, 1974).
- [11] C. Ciraci, Current-dependent potential for nonlocal absorption in quantum hydrodynamic theory, *Phys. Rev. B* **95**, 245434 (2017).
- [12] P. Ruggiero, P. Calabrese, B. Doyon, and J. Dubail, Quantum generalized hydrodynamics, *Phys. Rev. Lett.* **124**, 140603 (2020).
- [13] S. E. Kuratov, D. S. Shidlovski, and S. I. Blinnikov, Quantum shell effects in compressed mesoscopic system, *Phys. Plasmas* **26**, 022709 (2019).
- [14] S. E. Kuratov, D. S. Shidlovski, S. I. Blinnikov, and S. Yu. Igashov, Two scales of quantum effects in a mesoscopic system of degenerate electrons, *Phys.-Usp.* **64**, 836 (2021).
- [15] B. Ebeling, W. Kreft, and D. Kremp, *Theory of Bound States and Ionization Equilibrium in Plasma and Solids* (Mir, Moscow, 1979).
- [16] P. K. Shukla and B. Eliasson, Nonlinear aspects of quantum plasma physics, *Phys.-Usp.* **53**, 51 (2010).
- [17] N. Chakrabarti, J. S. Mylavarapu, M. Dutta, and M. Khan, Nonlinear interaction of quantum electron plasma waves with quantum electron acoustic waves in plasmas, *Phys. Rev. E* **83**, 016404 (2011).
- [18] R. Schmidt, B. J. B. Crowley, J. Mithen, and G. Gregori, Quantum hydrodynamics of strongly coupled electron fluids, *Phys. Rev. E* **85**, 046408 (2012).
- [19] M. Akbari-Moghanjoughi and P. K. Shukla, Theory for large-amplitude electrostatic ion shocks in quantum plasmas, *Phys. Rev. E* **86**, 066401 (2012).
- [20] P. K. Shukla and M. Akbari-Moghanjoughi, Hydrodynamic theory for ion structure and stopping power in quantum plasmas, *Phys. Rev. E* **87**, 043106 (2013).
- [21] I. S. Elkamash, I. Kourakis, and F. Haas, Ion-beam-plasma interaction effects on electrostatic solitary wave propagation in ultradense relativistic quantum plasmas, *Phys. Rev. E* **96**, 043206 (2017).
- [22] C. L. Gardner, The quantum hydrodynamic model for semiconductor devices, *SIAM J. Appl. Math.* **54**, 409 (1994).
- [23] A. Jungel, A note on current-voltage characteristics from the quantum hydrodynamic equations for semiconductors, *Appl. Math. Lett.* **10**, 29 (1997).
- [24] A. Unterreiter, The thermal equilibrium solution of a generic bipolar quantum hydrodynamic model, *Commun. Math. Phys.* **188**, 69 (1997).
- [25] G. B. Whitham, *Linear and Nonlinear Waves* (John Wiley & Sons, Hoboken, NJ, 1999).
- [26] S. E. Kuratov, D. S. Shidlovski, I. S. Menshov, and S. I. Blinnikov, Quantum shell effects in the hydrodynamic equations of quantum fluid, *J. Phys.: Conf. Ser.* **1238**, 012037 (2019).
- [27] S. Y. Gus'kov, J. Limpouch, P. Nicola, and V. T. Tikhonchuk, Laser-supported ionization wave in under-dense gases and foams, *Phys. Plasmas* **18**, 103114 (2011).
- [28] F. Pérez, J. D. Colvin, M. J. May, S. Charnvanichborikarn, S. O. Kucheyev, T. E. Felter, and K. B. Fournier, High-power laser interaction with low-density C–Cu foams, *Phys. Plasmas* **22**, 113112 (2015).